Unusual Roles of Secretory SNARE SYP132 in Plasma Membrane H$^+$-ATPase Traffic and Vegetative Plant Growth[1][OPEN]

Lingfeng Xia, Maria Mar Marquès-Bueno,[2] Craig Graham Bruce, and Rucha Karnik[3,4]

Plant Science Group, Laboratory of Plant Physiology and Biophysics, Institute of Molecular, Cell, and Systems Biology, University of Glasgow, Glasgow G12 8QQ, United Kingdom

ORCID IDs: 0000-0002-8628-8062 (L.X.); 0000-0003-3178-1922 (M.M.M.-B.); 0000-0002-3655-7535 (C.G.B.); 0000-0001-6876-4099 (R.K.).

The plasma membrane proton (H$^+$)-ATPases of plants generate steep electrochemical gradients and activate osmotic solute uptake. H$^+$-ATPase-mediated proton pumping orchestrates cellular homeostasis and is a prerequisite for plastic cell expansion and plant growth. All evidence suggests that the population of H$^+$-ATPase proteins at the plasma membrane reflects a balance of their roles in exocytosis, endocytosis, and recycling. Auxin governs both traffic and activation of the plasma membrane H$^+$-ATPase proteins already present at the membrane. As in other eukaryotes, in plants, SNARE-mediated membrane traffic influences the density of several proteins at the plasma membrane. Even so, H$^+$-ATPase traffic, its relationship with SNAREs, and its regulation by auxin have remained enigmatic. Here, we identify the Arabidopsis (*Arabidopsis thaliana*) Qa-SNARE SYP132 (Syntaxin of Plants132) as a key factor in H$^+$-ATPase traffic and demonstrate its association with endocytosis. SYP132 is a low-abundant, secretory SNARE that primarily localizes to the plasma membrane. We find that *SYP132* expression is tightly regulated by auxin and that augmented SYP132 expression reduces the amount of H$^+$-ATPase proteins at the plasma membrane. The physiological consequences of SYP132 overexpression include reduced apoplast acidification and suppressed vegetative growth. Thus, SYP132 plays unexpected and vital roles in auxin-regulated H$^+$-ATPase traffic and associated functions at the plasma membrane.

The P-type ATPase subfamily, plasma membrane proton (H$^+$)-ATPases, are among the most important ion pumps in plants. They extrude protons against an electrochemical gradient with the expenditure of ATP to generate strong proton motive forces that energize H$^+$-coupled transport and ion flux at the plasma membrane (Sze et al., 1999; Palmgren, 2001; Sondergaard et al., 2004). These plasma membrane H$^+$-ATPases drive various processes including osmotic nutrient uptake and stomatal opening, they facilitate salt tolerance and regulate intracellular pH, and they are essential for apoplast acidification and plastic cell wall loosening during vegetative growth (Sondergaard et al., 2004; Merlot et al., 2007; Palmgren et al., 2011).

Cell expansion is an essential process underlying plant growth and development. Growth begins with loosening of the rigid cell wall and an increase in turgor following osmotic water uptake. Secretory traffic delivers new membrane and wall materials for a growing cell (Cosgrove, 1987; Hager, 2003; Karnik et al., 2017). The long-standing acid-growth hypothesis attributes cell wall loosening and osmotic cell expansion to the activity of H$^+$-ATPases. Thus, for plant growth and homeostasis, the plasma membrane H$^+$-ATPases must be tightly regulated (Rayle and Cleland, 1970; Hager et al., 1971, 1991).

The phytohormone auxin triggers acid growth by activation of H$^+$ pumping, enhancing H$^+$-ATPase expression and affecting membrane traffic of the plasma membrane H$^+$-ATPases. Hager et al. (1991) noted a significant increase in membrane density of H$^+$-ATPases within few minutes of auxin treatment, attributed to membrane traffic, and demonstrated that a chemically

[1]This work was supported by the Royal Society (university research fellowship UF150364 and research grant RG160493 to R.K.). L.X. was supported by a Ph.D. scholarship from the China Scholarship Council. C.G.B. and M.M.M.-B. were supported by University of Glasgow Leadership funds to R.K.

[2]Present address: Department of Molecular Genetics, Centre for Research in Agricultural Genomics (CRAG), Campus Autonomous University of Barcelona (UAB), Edifici CRAG. Bellaterra - Cerdanyola del Vallès 08193 –Barcelona.

[3]Address for contact: rucha.karnik@glasgow.ac.uk.

[4]Senior author.

The author responsible for distribution of materials integral to the findings presented in this article in accordance with the policy described in the Instructions for Authors (www.plantphysiol.org) is: Rucha Karnik (rucha.karnik@glasgow.ac.uk).

R.K. conceived research plans and designed the experiments; R.K. and L.X. prepared constructs; M.M.M.-B., L.X., and R.K. did plant propagation and transgenic line preparation; R.K. and L.X. did the imaging experiments; M.M.M.-B and L.X. did RT-qPCR experiments; L.X. and R.K. did genotyping experiments; L.X. and R.K. did membrane partitioning experiments and immunoblots; L.X. did the yeast interaction assays; L.X., M.M.M.-B., and R.K. did plant phenotype experiments; R.K., L.X., and M.M.M.-B. analyzed data; C.G.B. provided technical assistance for all experiments; R.K. wrote the article with contributions from L.X.

[OPEN]Articles can be viewed without a subscription.

www.plantphysiol.org/cgi/doi/10.1104/pp.19.00266

induced block of protein synthesis diminished the auxin-enhanced density of H^+-ATPase proteins. In general, the density of membrane proteins is a balance between their forward traffic or exocytosis and their removal via endocytosis from the plasma membrane (Geldner et al., 2003). Therefore, different components of membrane traffic must accommodate the steady-state turnover as well as a more rapid, auxin-induced increase in the density of H^+-ATPase proteins at the plasma membrane. Thus, while the acid-growth hypothesis remains an important framework for understanding the role of auxin in cell expansion (Rayle and Cleland, 1970; Hager, 2003), it belies a simple interpretation in the context of posttranslational modifications.

More than two decades have passed since the acid-growth hypothesis established the importance of both membrane traffic and the functional activation of the H^+-ATPases. Yet, we know very little about the mechanisms underlying H^+-ATPase membrane traffic or about its tissue- and isoform-specific regulation. In Arabidopsis (*Arabidopsis thaliana*), three autoinhibited H^+-ATPase isoforms (AHA1, AHA2, and AHA11) are expressed throughout the plant (Harper et al., 1989; Palmgren, 2001; Arango et al., 2003). Among these, *AHA1* and *AHA2* together constitute almost 80% of H^+-ATPase mRNA transcripts and proteins (Haruta and Sussman, 2012). AHA1 and AHA2 show functional redundancy based on their transfer DNA (T-DNA) mutants (Haruta et al., 2010), even though recent studies suggest tissue-specific functions of AHA1 in the mediation of blue light responses and stomatal opening (Yamauchi et al., 2016).

Membrane proteins are usually synthesized in the endoplasmic reticulum and are trafficked through the Golgi, from which they are sorted to the plasma membrane, tonoplast, or other target membranes. Alternate forward trafficking pathways also exist that bypass the Golgi in plants (Di Sansebastiano et al., 2017). In all eukaryotes, secretory traffic to the plasma membrane is mediated by SNARE proteins. They also drive the traffic of membrane proteins and soluble cargo between various endomembrane compartments and the plasma membrane. The different subfamilies of SNARE proteins are classified by the presence of universally conserved Qa-, Qb-, Qc-, and R-SNARE amino acid motifs. Qa-SNAREs, commonly referred to as syntaxins, are generally located on the target membrane, while the R-SNAREs, also known as VAMPs (vesicle-associated membrane proteins), generally reside on the vesicle membrane (Jahn and Scheller, 2006). SNARE-mediated vesicle traffic occurs following assembly of the Qa- and R-SNAREs in a ternary SNARE complex with the Qb- and Qc-SNAREs, or the SNAP25-related (synaptosome-associated protein of 25 kD) Qbc-SNAREs, which draws the vesicle and target membranes in close proximity for fusion (Fasshauer et al., 1998; Bock et al., 2001).

In Arabidopsis, three Qa-SNAREs, SYP121 (Syntaxin of Plants121, or SYR1/PEN1) and its close homologs SYP122 and SYP132, are ubiquitously expressed at the plasma membrane throughout plant development (Enami et al., 2009). SYP132 expression makes up a minor portion of the Qa-SNAREs at the plasma membrane. Thus, together, SYP121 and SYP122 drive a bulk of secretory traffic to the plasma membrane (Tyrrell et al., 2007; Enami et al., 2009; Karnik et al., 2015). Distinct yet complementary pathways of SYP121- and SYP122- mediated secretory traffic affect vegetative plant growth (Karnik et al., 2015; Waghmare et al., 2018). Studies using dominant negative and mutant approaches showed that SYP121 and SYP122 do not affect plasma membrane H^+-ATPase traffic (Geelen et al., 2002; Sutter et al., 2006). Indeed, the SNARE regulatory protein, PATROL1, which is known to affect H^+-ATPase traffic, does not associate with SYP121 and SYP122 (Higaki et al., 2014). Thus, multiple lines of evidence discount any role of these two major Qa-SNAREs in H^+-ATPase traffic.

All the above observations leave unresolved the mechanism for H^+-ATPase traffic to and from the plasma membrane. Whether the plasma membrane H^+-ATPases are differentially regulated between plant tissues is also yet to be addressed. Using AHA1 as a model to study H^+-ATPase traffic together with the total H^+-ATPase population, here we report an unexpected role for the Qa-SNARE SYP132 (Enami et al., 2009; Ichikawa et al., 2014) in the regulation of density of the H^+-ATPase proteins at the plasma membrane of root and shoot epidermal cells. Remarkably, we find that modulating SYP132 expression affects clathrin-sensitive H^+-ATPase traffic from the plasma membrane, is subject to the hormone auxin, and influences apoplastic acidification and plant growth. Thus, we suggest that SYP132 and associated endocytosis are vital for plasma membrane H^+-ATPase traffic and play a major role in the physiology of plant growth and morphogenesis.

RESULTS

The Qa-SNAREs SYP111, SYP121, SYP122, and SYP132 are all expressed throughout the plant and form cognate SNARE complexes with the Qbc-SNARE SNAP33 and the R-SNAREs VAMP721 and VAMP722 (Enami et al., 2009; El Kasmi et al., 2013; Ichikawa et al., 2014). Both SYP111 (or KNOLLE) and SYP132 mediate vesicle traffic at the phragmoplast to support cytokinesis (Sanderfoot, 2007; Enami et al., 2009; Park et al., 2018). While SYP111 expression is cytokinesis specific, SYP132 occurs throughout plant development and likely has additional, yet undefined, roles in traffic at the plasma membrane. SYP132 has been implicated in plant-microbe interactions, the secretion of defense-related peptides at the plasma membrane, and basic plant growth (Catalano et al., 2007; Kalde et al., 2007; Enami et al., 2009; Limpens et al., 2009; Ichikawa et al., 2014; Huisman et al., 2016; Pan et al., 2016). However, like the *aha1/aha2* double mutant, T-DNA insertional mutants of *syp132* are embryo lethal (Park et al., 2018).

SYP132 Modulates AHA1 Localization at the Plasma Membrane

In the absence of a viable mutational strategy, we checked if SYP132 affects the cellular distribution of AHA1 by transiently coexpressing mCherry-AHA1 with GFP-fused SYP121 or SYP132 in tobacco (*Nicotiana tabacum*) leaf epidermi. This heterologous system has served as a useful model for initial studies involving Arabidopsis SNAREs and plasma membrane H+-ATPases in the past (Foresti et al., 2006; Sutter et al., 2006; Karnik et al., 2013; Zhang et al., 2015). Samples were treated with water before imaging (Fig. 1A). Additionally, for quantitative analysis, plasmolysis was induced (Supplemental Fig. S1) as an aide to resolve cell interior and to visualize the distribution of the fluorophore-fused proteins following retraction of the plasma membrane from the cell wall (Rafiqi et al., 2010).

The mCherry-AHA1 and GFP-SYP132 protein distribution at the cell periphery relative to the cell interior was determined by tracing around retracted cell periphery, region of interest (ROI) width ~1.5 μm, and the interior of each cell using the bright-field overlay for reference. Integrated fluorescence density within the ROIs marking the periphery and interior of each cell was measured, and corrected total fluorescence for each ROI was calculated following background subtraction (Marwaha and Sharma, 2017). When coexpressed with GFP-SYP132, the periphery-internal corrected total fluorescence ratio for mCherry-AHA1 was lower compared with when mCherry-AHA1 was expressed on its own or with GFP-SYP121 (Fig. 1D). These data show that coexpression of GFP-SYP132 leads to an increase in the proportion of mCherry-AHA1 present inside the cells, while the proportion of mCherry-AHA1 at the cell periphery is reduced.

SYP132 Affects AHA1 Internalization from the Plasma Membrane

To determine the effect of blocking SYP132 function on H+-ATPase density, a dominant negative fragment strategy was employed. In this case, we used a soluble fragment of the Qa-SNARE, SYP132$^{Habc\Delta}$, which lacks the conserved H3 domain containing the Qa-SNARE motif as well as the transmembrane domain (Supplemental Fig. S4, A–E). Together, both domains of the Qa-SNARE are necessary for vesicle fusion and secretory traffic at the plasma membrane (Geelen et al., 2002; Sutter et al., 2006; Karnik et al., 2013). The Qa-SNARE$^{Habc\Delta}$ or the so-called Sp3 fragments retain the interactive surfaces associated with cognate partner binding; however, they lose interactions with high-M_r regulatory proteins and ion transporters (Kargul et al., 2001). We used the yeast GPI signal peptide-anchored split-ubiquitin (GPS) system, which allows detection of soluble bait protein binding (Zhang et al., 2018), to test interactions of SYP132$^{Habc\Delta}$. We observed that SYP132$^{Habc\Delta}$ retains one-to-one binding with the cognate SNAREs SNAP33 or VAMP721 and with the full-length SYP132 (Supplemental Fig. S4). These interactions of SYP132$^{Habc\Delta}$ were similar to those of SYP132$^{\Delta C}$ (Supplemental Fig. S4), the conventional dominant negative or so-called Sp2 fragment, which lacks the C-terminal transmembrane domain (Sutter et al., 2006; Karnik et al., 2013, 2015, 2017; Grefen et al., 2015).

Additionally, the dominant negative effect of SYP132$^{Habc\Delta}$ in blocking secretory traffic at the plasma membrane was verified by assaying the traffic of cargoes that are known to be secreted. This technique (Waghmare et al., 2018) yields increased intracellular fluorescence if a fluorophore-fused secretory cargo accumulates within the secretory pathway due to the block of its traffic. The accumulation is quantified relative to the fluorescence of a nonsecretory marker that is expressed at the same time. The cargoes were each fused with mCherry and coexpressed with the GFP protein fused with an endoplasmic reticulum-retention HDEL motif (GFP-HDEL) using a tricistronic vector (Supplemental Fig. S5A) that ensures equal genetic loads on transformation. GFP-HDEL is retained in the endoplasmic reticulum and serves as a marker for transformation and for ratiometric fluorescence analysis of the block of secretion in the assay (Karnik et al., 2013; Waghmare et al., 2018). The CO_2 Response Secreted Protease (SBT5.2) is a SYP132-dependent cargo and is secreted independent of the SYP121 and SYP122 nexus (Waghmare et al., 2018). In the presence of SYP132 wild type, the mCherry-GFP ratio for mCherry-SBT5.2 was considerably lower compared with that of the nonsecreted mCherry (control), indicating secretion of this cargo. However, in the presence of SYP132$^{Habc\Delta}$, the mCherry-GFP ratio for mCherry-SBT5.2 was comparable to that of the nonsecreted control (Supplemental Fig. S5B). These data showed that secretion of the mCherry-SBT5.2 is reduced in the presence of SYP132$^{Habc\Delta}$. The secretion of the SYP132-independent cargo mCherry-Meristem5 (MERI-5; Waghmare et al., 2018) was not affected by SYP132 wild type, and only a marginal effect was observed in the presence of SYP132$^{Habc\Delta}$ (Supplemental Fig. S5), plausibly a consequence of titrating the cognate SNAREs that are shared between SYP121, SYP122, and SYP132. Thus, SYP132$^{Habc\Delta}$ acts as dominant negative and its overexpression blocks SYP132-dependent secretory traffic to the plasma membrane.

We anticipated that inducing constitutive overexpression of SYP132$^{Habc\Delta}$ would interfere with SYP132-mediated secretory traffic to the plasma membrane with specificity (Tyrrell et al., 2007). Surprisingly, however, following overexpression of the dominant-negative GFP-SYP132$^{Habc\Delta}$, the cell periphery-internal fluorescence ratio for mCherry-AHA1 increased compared with mCherry-AHA1 expressed on its own or with GFP-SYP132 or GFP-SYP121 (Fig. 1D). These data showed that mCherry-AHA1 localization to the cell periphery is augmented in the presence of the dominant negative GFP-SYP132$^{Habc\Delta}$.

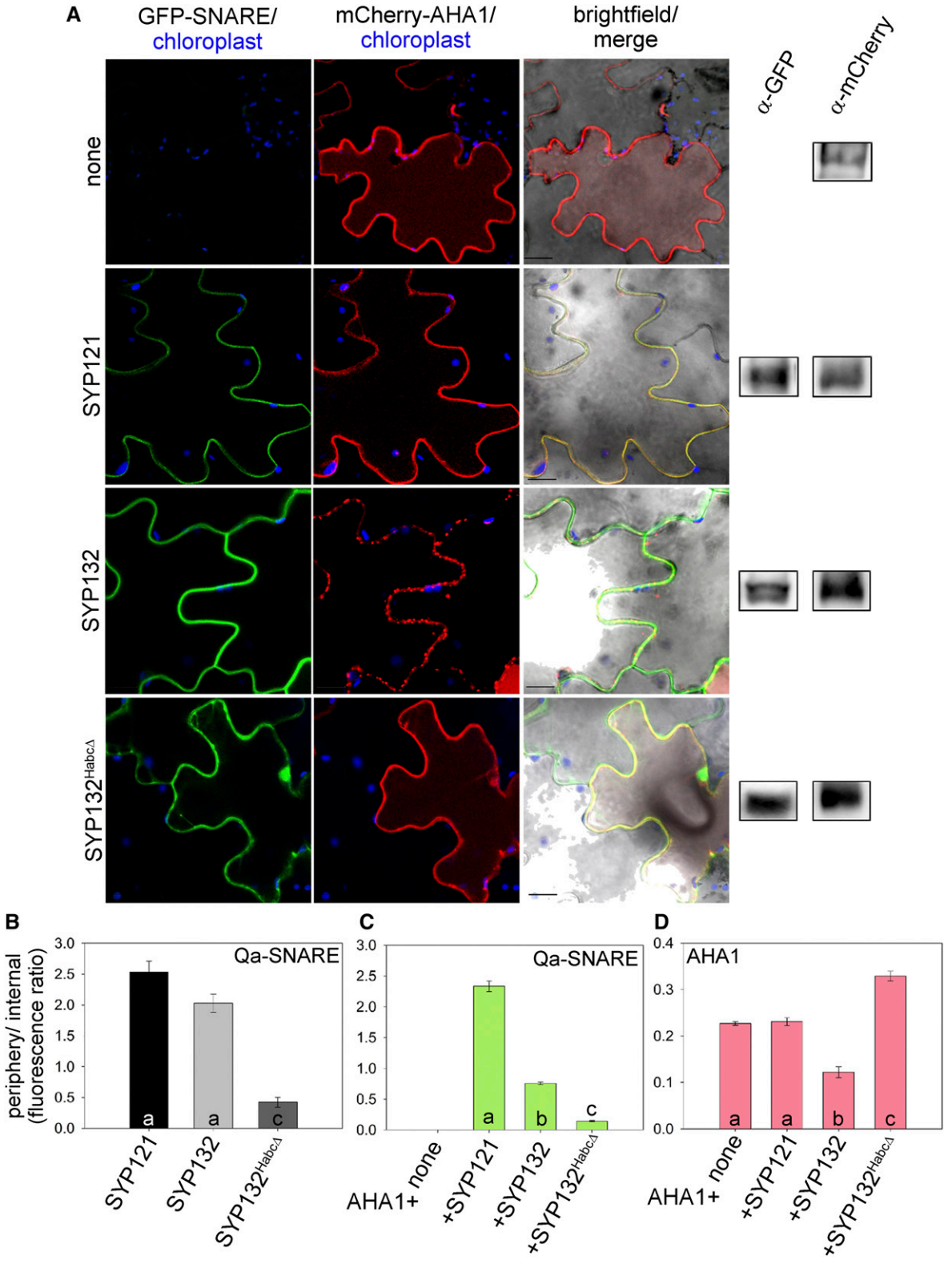

Figure 1. Effects of plasma membrane Qa-SNAREs on cellular AHA1 localization. A, Localization patterns in tobacco epidermal cells transiently transformed using the bicistronic pFRET-2in1gc-NN vector to express mCherry-fused AHA1 on its own or with GFP-fused Qa-SNAREs SYP121, SYP132, and SYP132^{HabcΔ}. Confocal images of the epidermal cells were acquired on a single focal plane. Representative (left to right) images show fluorescence for GFP-Qa-SNARE (green) overlay with chlorophyll (blue), mCherry-AHA1 (red) with chlorophyll (blue), and overlay with bright field. Immunoblots at right verify the expression of the

As controls, each of the full-length Qa-SNAREs were expressed in tobacco leaf epidermis. Confocal images showed that when expressed on their own, both SYP121 and SYP132 proteins are predominantly localized at the cell periphery (Fig. 1B; Supplemental Fig. S3). As anticipated for a soluble Qa-SNARE fragment, SYP132$^{Habc\Delta}$, the periphery-internal fluorescence ratio for red fluorescent protein (RFP)-SYP132$^{Habc\Delta}$ was significantly lower compared with the RFP-SYP132 (Fig. 1B; Supplemental Fig. S3), suggesting that the SYP132$^{Habc\Delta}$ fragment is localized to the cell interior.

Notably, compared with the SYP132 expressed on its own, the periphery-internal fluorescence ratio for GFP-SYP132 was lower when the Qa-SNARE was coexpressed with mCherry-AHA1. However, the cellular distribution of SYP121 was not affected by AHA1 coexpression (Fig. 1, A–C; Supplemental Fig. S3).

To test the specificity of SYP132 action, the Qa-SNARE was coexpressed with the K^+ channel KAT1. KAT1 delivery to the plasma membrane is affected in the *syp121* mutant plants (Eisenach et al., 2012), and mobility of the channel proteins within the plasma membrane is altered in the presence of the dominant negative fragment of SYP121 (Sutter et al., 2006, 2007). Confocal images of tobacco epidermal cells and their analysis showed that GFP-SYP132 has no effect on the distribution of mCherry-KAT1 puncta at the cell periphery or on their mobility. As expected, GFP-SYP121 altered mCherry-KAT1 distribution at the cell periphery (Supplemental Fig. S6). These data suggest that the SNARE SYP132 has distinct roles associated with AHA1 traffic within the cell.

To confirm if SYP132 affects H^+-ATPase integration at the plasma membrane in different cell types, 3-d-old Arabidopsis seedlings stably expressing 35S:GFP-AHA1 (Hashimoto-Sugimoto et al., 2013) were transiently transformed with RFP-fused SYP121, SYP132, and SYP132$^{Habc\Delta}$. Root hairs are single cells that are easy to isolate visually with a clear demarcation of cell interior, the plasma membrane, and outside of the cell. Therefore, confocal images of root hairs were acquired following labeling of the plasma membrane with lipophilic FM4-64 dye on ice (Fig. 2A). As a measure of integration of GFP-AHA1 into the plasma membrane, line scans across the plasma membrane were analyzed (Fig. 2, B and C) to determine the overlap of GFP-AHA1 with FM4-64 fluorescence signals as a percentage of the total FM4-64 signal across each line scan. A higher percentage total overlap with FM4-64 fluorescence in such analysis is therefore indicative of greater localization to the plasma membrane (Sklodowski et al., 2017). GFP-AHA1 expressed on its own (control) showed 85% ± 3% fluorescence overlap with FM4-64, akin to coexpression with RFP-SYP121. However, when coexpressed with RFP-SYP132, the overlap of GFP-AHA1 with FM4-64 was significantly lower and, conversely, coexpression with the RFP-SYP132$^{Habc\Delta}$ increased GFP-AHA1 overlap with FM4-64 (Fig. 2C). Thus, abrogation of SYP132 function using the dominant negative SYP132$^{Habc\Delta}$ enhanced GFP-AHA1 localization at the plasma membrane.

It is notable that in transiently transformed cells, fluorophore-fused AHA1 appeared to localize in punctate structures in the interior of cells coexpressing SYP132 (Figs. 1–3; Supplemental Fig. S1). Similarly, GFP-AHA1 appeared in punctate structures within the interior of stomatal guard cells (Supplemental Fig. S7, A and C) and root hairs (Supplemental Fig. S6, B and C) in Arabidopsis stable lines coexpressing RFP-SYP132 under the control of the constitutive 35S promoter (Supplemental Fig. S7C). Together, these data demonstrate that SYP132 affects AHA1 localization within the cell in different tissue types and in both transient and stable systems.

SYP132-Associated H^+-ATPase Traffic Is Sensitive to Clathrin-Mediated Endocytosis

Previous studies had noted that plasma membrane H^+-ATPases accumulate in endosomal structures in some circumstances (Kitakura et al., 2011). Such H^+-ATPase traffic within the cells has been attributed to be clathrin-mediated endocytosis (CME) from the plasma membrane (Dhonukshe et al., 2007). To test if SYP132 causes AHA1 redistribution to intracellular compartments (Fig. 2A), possibly as a result of clathrin-mediated endocytic traffic, we used the clathrin H chain 1 mutant, *chc1*, and stable Arabidopsis lines of the tamoxifen-inducible dominant negative mutant HUB1, which are deficient in CME (Kitakura et al., 2011; Larson et al., 2017). Three-day-old wild-type and clathrin mutant Arabidopsis seedlings were transiently transformed to express mCherry-AHA1 on its own and together with GFP-SYP132. In parallel experiments, seedlings from the same lines were labeled with FM4-64 and analyzed for internalization to ensure that the block of CME was observed in the transgenic lines compared with the wild-type seedlings (Gaffield and Betz, 2006). As a measure of internalization, mCherry-AHA1,

Figure 1. (*Continued.*)
Qa-SNAREs and AHA1 with anti-GFP and anti-mCherry antibodies, respectively (see Supplemental Fig. S2A). Bars = 20 μm. B to D, Bar graphs show mean cell peripheral-internal fluorescence ratios ± SE ($n \geq 12$) for Qa-SNAREs (RFP fused) expressed on their own (B; see Supplemental Fig. S3), for Qa-SNAREs (GFP fused) coexpressed with AHA1 (C), and for AHA1 (mCherry fused) expressed on its own (none) or with the Qa-SNAREs (D). Cells were plasmolyzed with 1 M NaCl to retract the plasma membrane and resolve the cell interior. Images were collected as Z-stacks and rendered as 3D projections (Supplemental Fig. S1) prior to analysis. The region of the cell periphery, ~1.5 μm in width, and the cell interior were traced for each cell using the bright-field image as a reference. Integrated fluorescence density within the ROIs was measured and corrected for background fluorescence (see "Materials and Methods"). Statistically significant differences using ANOVA are indicated with different letters ($P < 0.001$).

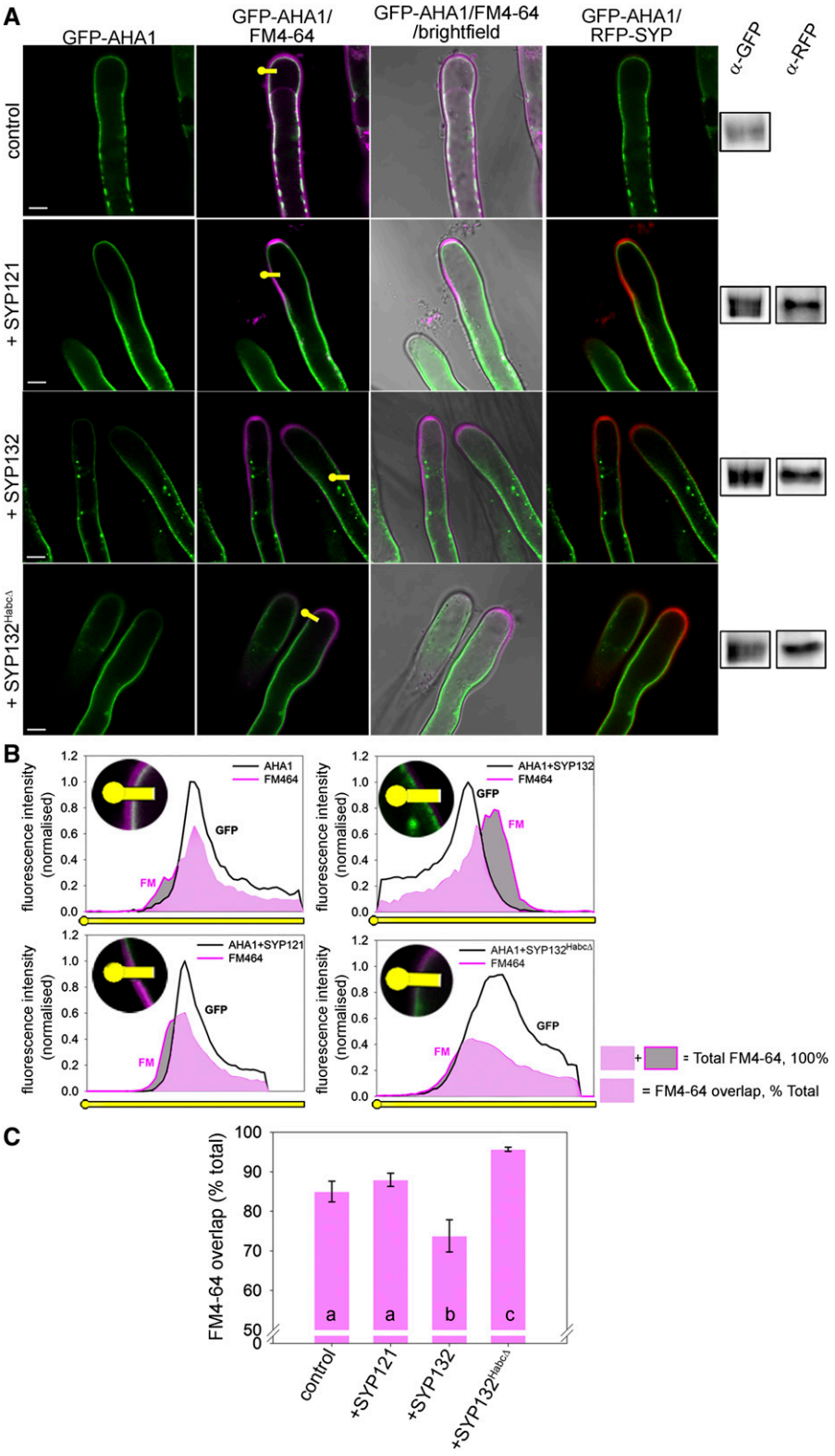

Figure 2. SYP132 affects AHA1 integration into the plasma membrane. A, Localization patterns in root hairs from 3-d-old 35S:*GFP-AHA1* Arabidopsis seedlings (Hashimoto-Sugimoto et al., 2013) stably expressing GFP-AHA1 were transformed with empty vector (control) or RFP-fused SYP121, SYP132, and SYP132$^{Habc\Delta}$ under the control of the *Cauliflower mosaic virus* (CaMV) 35S promoter (Karimi et al., 2002) and stained with 3 μM FM4-64 (5 min on ice) to label the plasma membrane. Seedlings were washed in growth medium prior to imaging. Representative single-plane confocal images of root hairs show (left to right) florescence for GFP-AHA1 (green), GFP-AHA1 (green) overlay with FM4-64 (pink), GFP-AHA1 (green) and FM4-64 (pink) overlay with bright field, and the GFP-AHA1 (green) overlay with RFP-SYP (red; ~7% bleedthrough from FM4-64). Immunoblots at right verify the expression of GFP-AHA1 and the RFP-SYPs using anti-GFP and anti-RFP antibodies, respectively (see Supplemental Fig. S2B). Yellow lollipops mark representative regions of the root hair membrane across which fluorescence intensities for GFP (black lines) and FM4-64 (pink lines) were plotted (Sklodowski et al., 2017). Bars = 5 μm. B, Plots of GFP-AHA1 and FM4-64 fluorescence overlap in the line scan across the membrane, represented by the yellow lollipop in A. Round insets are enlarged sections of the root hair image in A, marking a representative line scan region. Peak areas shaded pink represent FM4-64 and GFP-AHA1 overlap, and gray areas with pink outlines represent lack of FM4-64 overlap, represented schematically at bottom right. C, Bar graphs plot the percentage of total FM4-64 that overlaps with GFP-AHA1. Plots are mean values ± SE from 20 or more root hairs. Statistically significant differences using ANOVA are indicated with letters ($P < 0.0.05$).

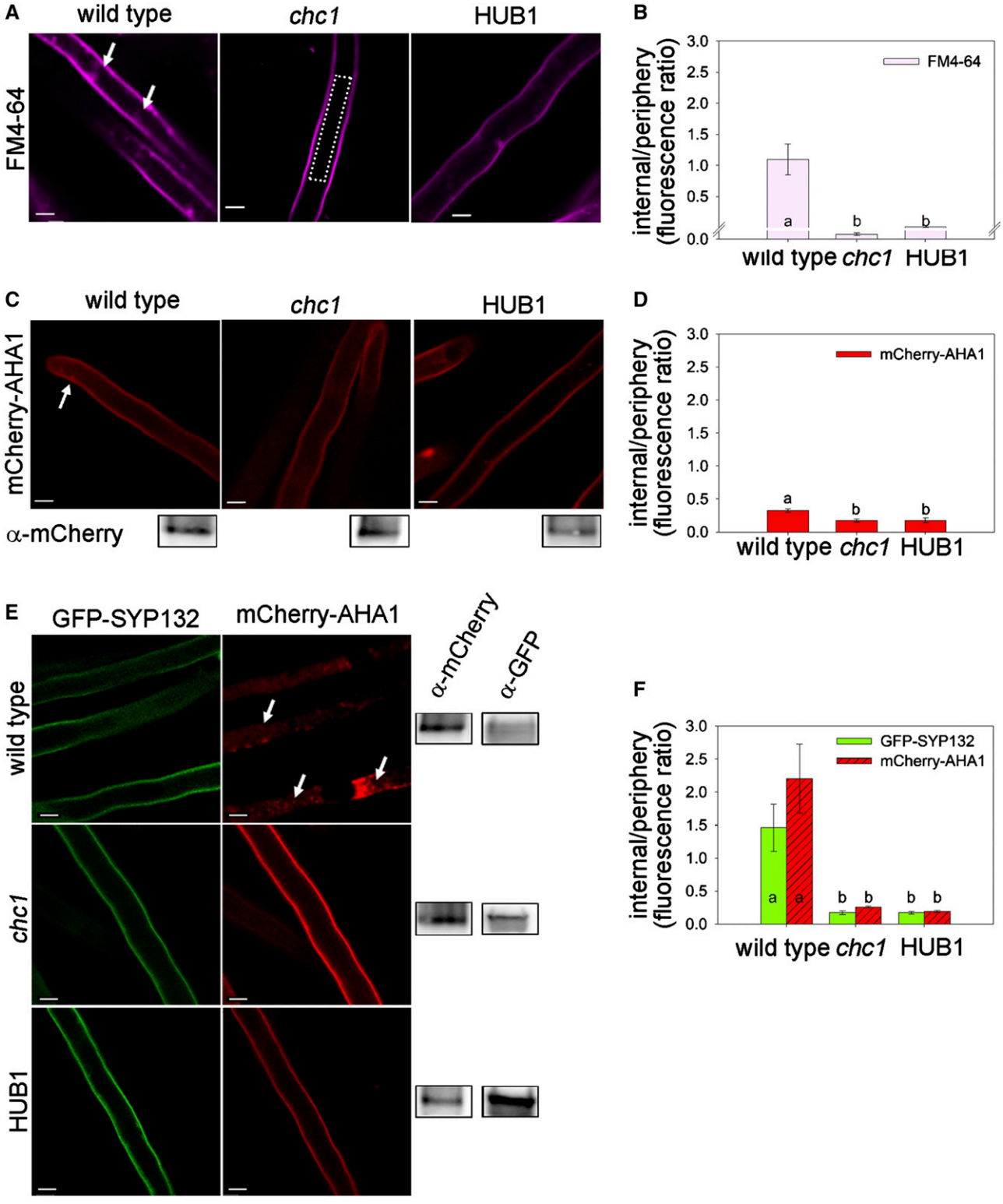

Figure 3. Block of clathrin function perturbs SYP132-associated internalization of AHA1. A, C, and E, Representative confocal images of root hairs from wild-type and clathrin mutant Arabidopsis lines *chc1* and HUB1 (+2 μM hydroxytamoxifen, for 48 h). Images represent florescence of FM4-64 (pink), mCherry-AHA1 (red), and GFP-132 (green). White arrows mark intracellular accumulation. Bars = 5 μm. A, At the plasma membrane, to test for endocytosis in the wild-type seedlings and block of CME in the *chc1* and HUB1 lines, seedlings were stained with 3 μM FM4-64 for 5 min and washed in growth medium prior to imaging after 30 min. C and E, Wild-type, *chc1*, and HUB1 seedlings were transiently transformed using the pFRET-2in1gc-NN vector to

GFP-SYP132, or FM4-64 distribution at cell periphery and interior was analyzed in the root hair cells. An outline was drawn around the cell interior and along the cell periphery, and mean fluorescence was measured (Fig. 3A). The ratio of internal to periphery fluorescence following subtraction of background fluorescence (see "Materials and Methods") was calculated, and mean fluorescence ratios were plotted (Fig. 3, B, D, and F). In the *chc1* and HUB1 seedlings, FM4-64 uptake into the cell interior was reduced compared with that in wild-type seedlings, thus confirming the block of CME (Fig. 3, A and B). In parallel experiments, when expressed on its own, mCherry-AHA1 showed marginal internalization in wild-type root hair and in the clathrin mutant seedlings (Fig. 3, C and D). However, in seedlings where mCherry-AHA1 was coexpressed with GFP-SYP132, the internal-periphery fluorescence ratio was considerably higher for both mCherry-AHA1 and GFP-SYP132 in the wild-type Arabidopsis root hair but not in the clathrin mutant lines (Fig. 3, E and F). Together, these data suggest that SYP132-associated redistribution of the H^+-ATPase proteins from the plasma membrane to intracellular compartments is sensitive to clathrin.

SYP132 Affects H^+-ATPase Redistribution from the Plasma Membrane

mCherry-AHA1 internalization was observed only after coexpression of GFP-SYP132 (Fig. 3; Supplemental Fig. S7), although native SYP132 was present. In each of these experiments, GFP-SYP132 was constitutively overexpressed under the control of the CaMV 35S promoter. Therefore, we asked if H^+-ATPase traffic was linked to the levels of SYP132 expression. To augment SYP132 expression, wild-type Arabidopsis was stably transformed (SYP132-OX) to constitutively overexpress GFP- or RFP-fused SYP132 proteins. Two independent SYP132-OX lines that showed similar levels of fluorophore-fused SYP132 protein expression in the T3 generation (Supplemental Fig. S8A) were chosen for experiments. Driven by the CaMV 35S promoter, the SYP132-OX lines showed roughly a 13-fold higher expression, while in the heterozygous *syp132* mutant (*syp132*^{T}; Park et al., 2018; Supplemental Fig. S8B), expression was reduced by 5-fold lower when compared with the wild-type plants (Supplemental Fig. S8C).

To measure intracellular distribution of the H^+-ATPase proteins in each of these lines, Arabidopsis leaf microsomes were isolated and used to separate plasma membrane and internal membrane fractions, utilizing the aqueous two-polymer phase system (Yoshida et al., 1983; Sutter et al., 2007). Proteins in the plasma membrane and internal membrane fractions were resolved by SDS-PAGE followed by immunoblot analysis. Purity of the enriched fractions was determined to be ~95% by immunoblot analysis using antibodies against the KAT1 K^+ channel as a marker for the plasma membrane fraction and against the endoplasmic reticulum-resident lumen-binding protein BiP as a marker for the total internal membrane fraction. Immunoblot analysis was carried out using anti-RFP (or anti-GFP) antibodies to detect the RFP- (or GFP)-fused SYP132 to detect distribution of this SNARE in the plasma membrane and internal membrane fractions. Immunoblot analysis using native Arabidopsis anti-H^+-ATPase antibodies, which bind all isoforms of the AHAs (Fig. 4A), detected total H^+-ATPase protein population in the membrane fractions. Immunoblot band intensities were analyzed by densitometry and normalized to the total protein for each gel lane. The quantity of H^+-ATPase proteins, relative to wild-type leaves, was thus calculated and plotted (Fig. 4, B–D). We found that the density of the H^+-ATPase proteins at the plasma membrane when compared with the wild-type leaves was 2-fold higher in *syp132*^{T} leaves while it was 2-fold lower in the SYP132-OX leaves. In SYP132-OX leaves, the majority of the H^+-ATPase proteins were localized to the internal membranes (Fig. 4, A and B). Total H^+-ATPase protein density in microsomes was higher in the *syp132*^{T} leaves, but there was no obvious difference in total H^+-ATPase protein density between wild-type and SYP132-OX leaves (Fig. 4C). A significant proportion of the RFP-SYP132 proteins were also localized to the internal membranes (Fig. 4D). Together, these data suggest that SYP132 affects total H^+-ATPase protein distribution to the plasma membrane.

Modulation of SYP132 Expression Affects Acid Growth

Given that SYP132 affected H^+-ATPase protein density at the plasma membrane, we examined whether changes in this density translated to net H^+-ATPase activity at the plasma membrane. As a measure of H^+ extrusion, the mean pH of the apoplast was measured by water infiltration and centrifugation. Rosette leaves of 3-week-old wild-type, *syp132*^{T}, and SYP132-OX plants were infiltrated, immediately cut into strips, placed in spin columns, and centrifuged to elute the apoplastic wash fluid (Grefen et al., 2015). The pH of the

Figure 3. (*Continued.*)
express mCherry-fused AHA1 on its own (C) or with GFP-fused SYP132 (E). Bottom images in C and right images in E show immunoblots with anti-mCherry or anti-GFP antibodies to verify expression of AHA1 and SYP132, respectively (see Supplemental Fig. S2, C and D). B, D, and F, Graphs represent mean internal versus peripheral fluorescence ratio following background subtraction. The region along the cell periphery, ~1.5 μm in width, and the cell interior were traced for each cell using the bright-field image as a reference. The representative region for internal fluorescence measurement is shown with a white dotted line in A, middle image. Measurements were obtained for FM4-64 (B), mCherry-AHA1 (D), and GFP-SYP132 or mCherry-AHA1 (F). Mean values ± SE are plotted from $n \geq 20$ root hairs. Letters indicate statistically significant differences using ANOVA ($P < 0.001$).

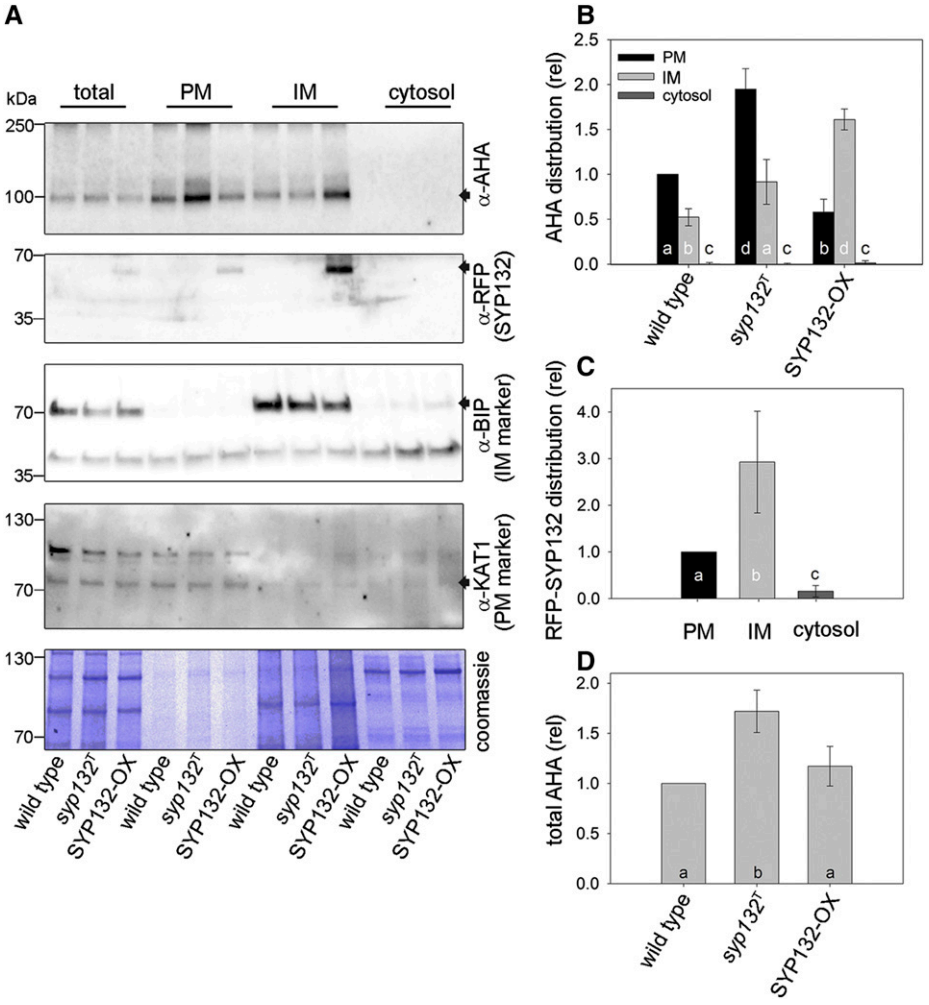

Figure 4. SYP132 overexpression relocalizes plasma membrane H+-ATPases into internal membranes. A, Immunoblots of microsomal membrane (total), plasma membrane (PM), internal membrane (IM), and soluble (cytosol) fractions purified (see "Materials and Methods") from rosette leaves of wild-type, *syp132*^{T}, and SYP132-OX Arabidopsis. Proteins were resolved on a single gradient gel (4% to 20% polyacrylamide SDS-PAGE), and specific proteins were visualized by immunoblots using antibodies: anti-H+-ATPase (AHA; ~95 kD; first gel), anti-RFP (RFP-SYP132; ~61 kD; second gel), anti-BiP (lumen-binding protein; ~73 kD; third gel), and anti-KAT1 (KAT1 K^+ channel; ~78 kD; fourth gel). Total protein for each gel lane detected using Coomassie blue stain (bottom gel) was used for quantitative analysis. Black lines (left) indicate positions of molecular mass markers, and black arrows (right) indicate expected band positions. Based on band intensities for KAT1, ~96% of the marker appeared in the plasma membrane fractions, and for BiP, ~95% of the marker appeared in the internal membrane fractions, suggesting membrane fraction purity in excess of 95%. B, Relative AHA distribution in the plasma membrane, internal membrane, and cytosol fractions of wild-type, *syp132*^{T}, and SYP132-OX leaves quantified from immunoblots using the Fiji software. C, Relative RFP-SYP132 distribution in plasma membrane, internal membrane, and cytosol fractions of SYP132-OX leaves. D, Relative AHA density in microsomal membranes (total AHA) of wild-type, *syp132*^{T}, and SYP132-OX Arabidopsis. Data are means ± SE from $n \geq 3$ independent experiments. Statistical significance using ANOVA is indicated by letters ($P < 0.05$).

apoplast wash fluid was measured using a calibrated micro pH electrode. Compared with the wild-type leaves, the mean apoplast wash fluid pH in SYP132-OX leaves was more alkaline, while in the *syp132*^{T} leaves, the pH was more acidic (Fig. 5A). Thus, modulation of SYP132 expression affected H+-ATPase density and net H+ extrusion at the plasma membrane.

To test whether changes in H+-ATPase density and net function affected plant growth, plant growth was measured as a function of rosette area, shoot fresh weight (Hashimoto-Sugimoto et al., 2013), and hypocotyl length. The various plant lines were cultivated under standard growth conditions for 3 weeks before growth above ground was assayed for shoot weight and rosette area. In addition, hypocotyl length was measured from seedlings following 4 d of growth in the dark. We found that the SYP132-OX plants exhibited a reduced aboveground shoot growth on soil compared with wild-type and *syp132*^{T} plants (Fig. 5, B–G). These experiments were repeated in four independently

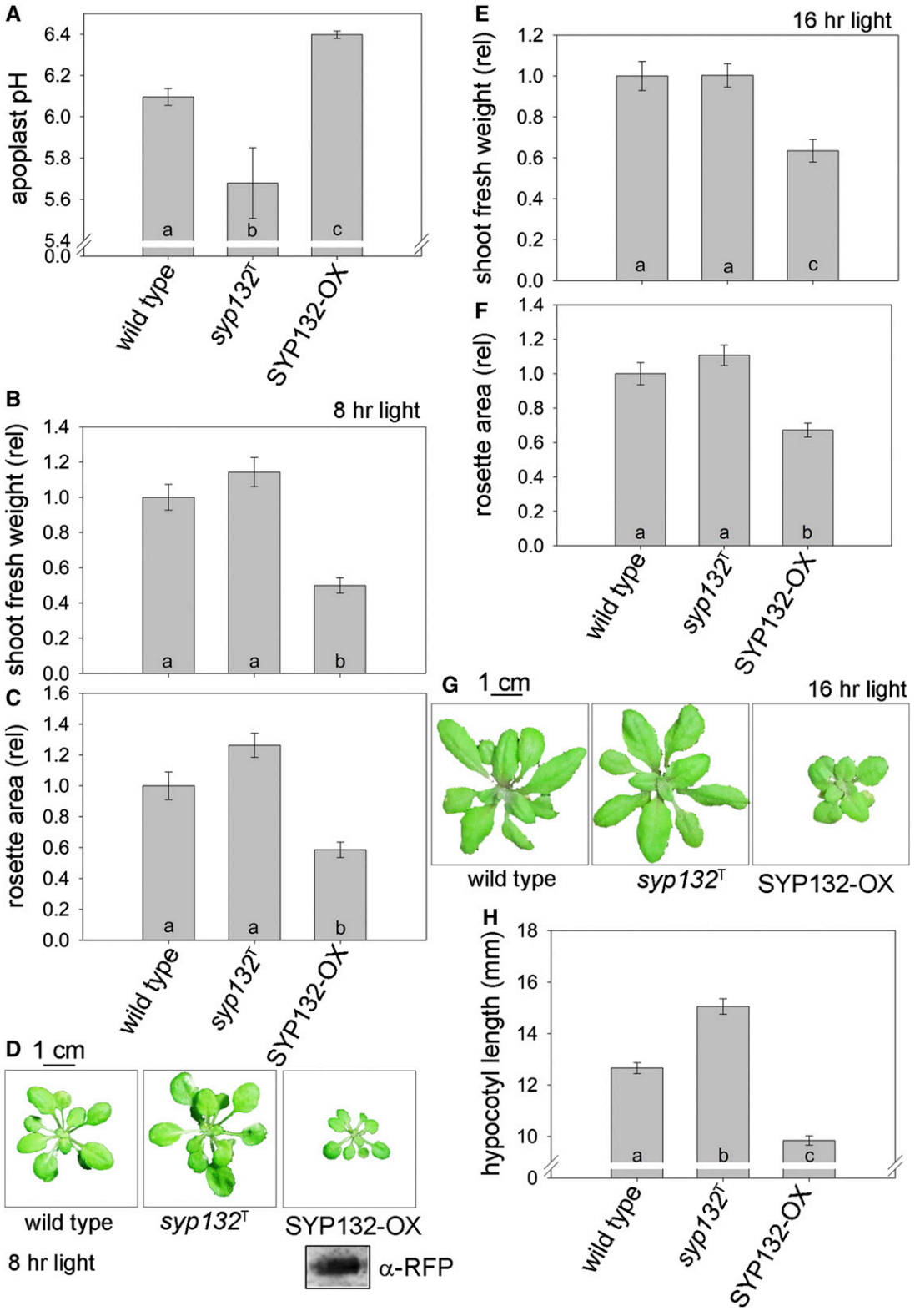

Figure 5. Modulation of SYP132 expression alters H^+-ATPase function and plant growth. A, pH of apoplast wash fluid eluted in water was measured (see "Materials and Methods") from 3-week-old wild-type, *syp132*^{T}, and SYP132-OX Arabidopsis leaves. Apoplast wash fluid from three different leaves from each plant was pooled, and pH was measured using a micro pH electrode. Data are means ± SE, $n \geq 10$ plants. Statistical significance using ANOVA is indicated by letters ($P < 0.05$). B and C, Mean ± SE values from 30 or more plants each of wild-type, *syp132*^{T}, and SYP132-OX Arabidopsis grown in 8 h of light for 3 weeks before

transformed transgenic SYP132-OX lines, and each exhibited similar phenotypes (Supplemental Fig. S9). As controls for this experiment, the SYP121-OX seedlings showed no significant differences in shoot growth compared with the wild-type seedling, while, as expected, the AHA1-OX shoots, which have increased population of the H+-ATPase proteins at the plasma membrane, grew bigger (Wang et al., 2014; Supplemental Fig. S10). Hypocotyl length in dark-grown SYP132-OX seedlings was shorter than in wild-type seedlings but longer in *syp132*^{T} seedlings (Fig. 5H; Supplemental Fig. S9D). Together, these data imply that changes in H+-ATPase protein density have direct implications on its function at the plasma membrane; an increase in density of the H+-ATPase proteins at the plasma membrane promotes plant growth.

Auxin Regulates Expression of the Low-Abundance Arabidopsis Qa-SNARE SYP132

The phytohormone auxin regulates both the activity and the density of H+-ATPase proteins at the plasma membrane (Hager et al., 1971; Hager, 2003), and its action is one of the key tenets of the acid-growth hypothesis. Since SYP132 overexpression negatively regulates H+-ATPase protein density and function, we set out to determine if auxin has a role in the modulation of *SYP132* expression.

Auxin promotes growth in both shoot and root tissues at low concentrations (10^{-11} M), but at higher concentrations of auxin (10^{-6} M), a temporal inhibition of primary root growth is observed, noticeably within 45 to 180 min of treatment (Evans et al., 1994; Velasquez et al., 2016). In shoots, auxin induces growth even at high concentrations (10^{-5} M or greater; Fendrych et al., 2016). Thus, 10^{-6} M 1-naphthyl-acetic acid auxin (NAA) has opposite effects on growth between root and shoot tissue. We exploited this auxin concentration dependence of plant growth to test if the hormone regulates SYP132 expression differentially between root and shoot for the promotion or suppression of plant growth.

To quantify root- and shoot-specific expression of *SYP132* transcripts in whole plant or separated roots and shoots, reverse transcription quantitative PCR (RT-qPCR) was carried out (Omelyanchuk et al., 2017). As a control subset, the transcript levels of *SYP121* and the root-specific *SYP123* were assessed (Bassham and Blatt, 2008; Ichikawa et al., 2014). Figure 6A shows the transcript levels for each of these Qa-SNAREs in whole plants. Supplemental Table S1 lists RT-qPCR primer-binding efficiencies, enabling transcript levels of the different SNAREs to be compared. These data confirmed that *SYP121* transcripts are higher by about 100-fold than *SYP123* and *SYP132* (Enami et al., 2009).

To determine the effect of auxin on Qa-SNARE expression, Arabidopsis seedlings were grown for 5 to 7 d on soft agar. The shoots were separated from roots at the hypocotyl junction prior to treatment with 10^{-6} M NAA for 60 and 180 min. No significant effects of auxin on the expression of *SYP121* and *SYP123* transcripts were observed; however, substantial differences were noted in the transcription of SYP132. Following auxin treatment, SYP132 transcripts decreased 2-fold in shoots (Fig. 6B), while they increased 3-fold in roots (Fig. 6C) compared with the control. Thus, in high concentrations of auxin that promote growth, SYP132 transcript levels are concurrently down-regulated in shoots. Conversely, for the same concentrations of auxin that suppress growth in roots, SYP132 transcript abundance is up-regulated. In other words, the transcription of SYP132 parallels the actions of auxin on growth between the root and shoot.

Modulation of SYP132 Expression Affects Stomatal Apertures

Stomatal opening depends on turgidity of the two stomatal guard cells: turgid guard cells hold open the stomatal pore and flaccid guard cells cause stomatal closure. Activation and membrane traffic of key transporters, including the H+-ATPases in the guard cell plasma membrane, is a major determinant of stomatal aperture regulation and its interaction with the environment (Kinoshita and Shimazaki, 1999; Eisenach et al., 2012; Hashimoto-Sugimoto et al., 2013; Yamauchi et al., 2016; Jezek and Blatt, 2017; Vialet-Chabrand et al., 2017).

To test if modulation of SYP132 and its impact on H+-ATPase traffic affects stomatal aperture, intact leaf stomatal apertures were measured in 4-week-old plants grown in 150 μmol m^{-2} s^{-1} photosynthetically active radiation (PAR) light (Chitrakar and Melotto, 2010) to compare the effects of SYP132 expression. We found that apertures in *syp132*^{T} plants were larger and, conversely, that apertures of SYP132-OX plants were smaller compared with the wild type (Fig. 7).

Figure 5. (*Continued.*)
measurement of shoot fresh weight (B) and rosette area (C). Values are normalized to the wild type, and statistical significance is indicated by letters ($P < 0.001$). D, Photographs of 3-week-old wild-type, *syp132*^{T}, and SYP132-OX Arabidopsis rosettes grown in 8 h of light. The immunoblot at bottom with anti-RFP antibodies verifies the expression of RFP-SYP132. Bar = 1 cm. E and F, Mean ± SE data of shoot fresh weight (E) and rosette area (F) from 30 or more 3-week-old wild-type, *syp132*^{T}, and SYP132-OX Arabidopsis grown in 16 h of light. Values are normalized to the wild type, and statistical significance is indicated by letters ($P < 0.05$). G, Three-week-old wild-type, *syp132*^{T}, and SYP132-OX Arabidopsis grown in 16 h of light. Images for rosettes were digitally extracted using ImageJ. Bar = 1 cm. H, Mean ± SE hypocotyl length in wild-type, *syp132*^{T}, and SYP132-OX Arabidopsis measured from 4-d-old dark-grown seedlings (30 or more). Independently transformed SYP132-OX lines all showed similar phenotypes (Supplemental Fig. S10). Statistical significance using ANOVA is indicated by letters ($P < 0.001$).

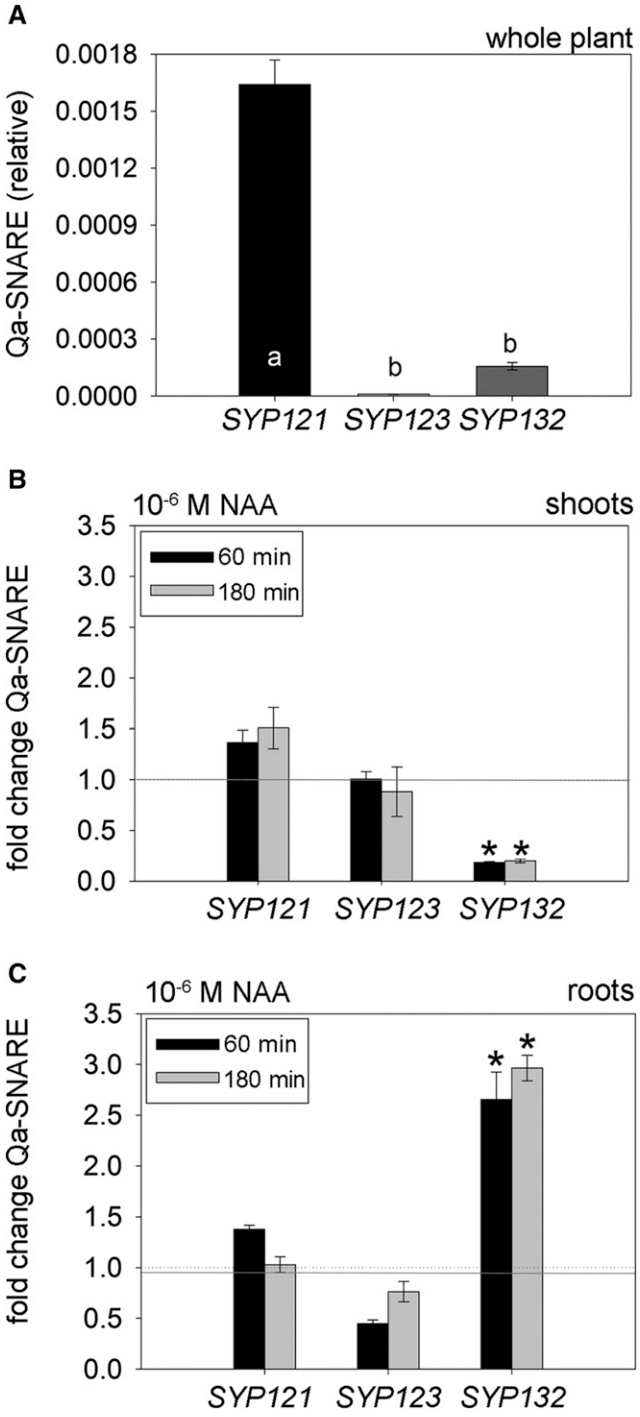

Figure 6. The phytohormone auxin regulates *SYP132* expression levels. RT-qPCR analysis is shown relative to mitochondrial 18s rRNA (AtMg01390) expression as a reference on whole plants or separated shoot and root tissue from 5- to 7-d-old Arabidopsis. A, Relative *SYP121*, *SYP123*, and *SYP132* expression ($2^{-\Delta CT}$) in shoot and root tissue. Data are means ± SE, representative of three biological replicates. Letters denote statistically significant differences determined using ANOVA ($P < 0.001$). B and C, Fold change in *SYP121*, *SYP123*, and *SYP132* expression ($2^{-\Delta\Delta CT}$; Livak and Schmittgen, 2001) compared with the control (0.02% [v/v] ethanol in water) upon treatment with 10^{-6} M NAA for 60 min (gray bars) and 180 min (black bars) in shoots (B) and roots (C). Mean values ± SE, representative of three biological replicates, are plotted. Asterisks indicate statistically significant differences compared with the control using Student's *t* test (*, $P < 0.001$); the fold change reference (1) is marked with a dotted line. Since the data were either not normally distributed or had unequal variances, a Kruskal-Wallis ANOVA on ranks was undertaken and a pairwise comparison using Dunn's method was applied.

As a primary transporter in stomatal guard cells, H+-ATPase activation occurs following posttranslational modifications of its C terminus. Phosphorylation of the C-terminal regulatory domain of the H+-ATPases facilitates the binding of 14-3-3 proteins and the release of autoinhibition (Palmgren, 2001). The fungal phytotoxin fusicoccin induces irreversible stomatal opening by stabilizing 14-3-3 protein binding and activation of the H+-ATPases (Marre, 1979; Fuglsang et al., 2003). Thus, we also compared apertures following treatments with fusicoccin. We found that the fungal toxin increased stomatal opening in all the plant lines including SYP132-OX (Fig. 7). Together, these data indicated that SYP132 negatively regulates stomatal aperture and that this effect of SYP132 can be rescued by treatment with fusicoccin.

Hormones and the Fungal Toxin Fusicoccin Affect SYP132-Associated H+-ATPase Traffic

The effects of fusicoccin treatment reflected in stomatal aperture measurements might be explained by enhanced activation of the H+-ATPases present at the plasma membrane in the SYP132-OX lines. For example, if 14-3-3 binding blocks SYP132-associated H+-ATPase traffic, it might thereby increase both the density and activity at the H+-ATPases at the plasma membrane. Alternatively, fusicoccin might augment H+-ATPase expression and lead to a proportionate increase in density and function of the pumps at the plasma membrane. To distinguish between these different possibilities, we carried out fractionation of microsomes prepared from leaves treated with control (0.02% [v/v] ethanol in water), 10^{-6} M NAA (auxin), and 10^{-5} M fusicoccin for 2 h (Hashimoto-Sugimoto et al., 2013). Auxin treatment in these experiments served as an experimental control for its effects on enhancing H+-ATPase activity at the plasma membrane. H+-ATPase and RFP-SYP132 populations in the plasma membrane and internal membrane fractions were estimated as a measure of the density of respective bands on immunoblots and normalized to the total protein for each gel lane. These H+-ATPase and RFP-SYP132 protein quantities were plotted relative to the wild-type, control treatment samples (Fig. 8A; Supplemental Fig. S11).

We found that NAA treatment led to significant increases in the H+-ATPase protein density in the plasma membrane. The plasma membrane-to-internal membrane ratio of H+-ATPase protein was higher in

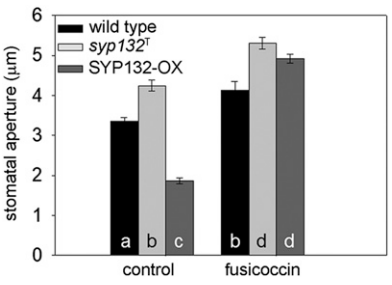

Figure 7. Modulation of SYP132 expression affects stomatal aperture. Steady-state, intact leaf stomatal aperture values are shown for 4-week-old wild-type, *syp132*^{T}, and SYP132-OX Arabidopsis following treatment with control (0.02% [v/v] ethanol in water) and 10^{-5} M fusicoccin for 2 h. Data are means ± SE from 100 or more stomata from three independent experiments measured using the Fiji (National Institutes of Health) software. Statistical significance using ANOVA is indicated by letters ($P < 0.05$).

wild-type plants treated with NAA compared with the control (Fig. 8D). Indeed, Hager et al. (1991) had noted an increase in plasma membrane density of the H+-ATPases following auxin treatment in maize (*Zea mays*) coleoptiles. In the SYP132-OX leaves, NAA did not have any obvious effects on the distribution of the H+-ATPases between the plasma membrane and endosomal compartments (Fig. 8, A, B, and D).

Following fusicoccin treatment, H+-ATPase protein density increased in purified plasma membrane fractions from leaves of both wild-type and SYP132-OX plants compared with the control (Fig. 8, A, B, D, and F). Total H+-ATPase protein levels also showed a significant increase in wild-type and SYP132-OX leaves following fusicoccin treatment compared with the control (Fig. 8F). In the SYP132-OX leaves, the plasma membrane-to-internal membrane ratio of the H+-ATPase protein levels increased in fusicoccin-treated leaves compared to the control, although the total H+-ATPase protein density was lower than in the wild-type leaves. Thus, fusicoccin promoted an increase in H+-ATPase protein density at the plasma membrane compared with the internal compartments, thereby reversing the effect of SYP132-OX. Corresponding to H+-ATPase proteins, the plasma membrane density of RFP-SYP132 also increased in fusicoccin-treated leaves compared with the control and NAA (Fig. 8C). Therefore, we conclude that fusicoccin increases both total cellular and plasma membrane H+-ATPase protein populations in wild-type and SYP132-OX plants.

To test how plasma membrane H+-ATPase protein distribution at the plasma membrane is regulated by a hormone that suppresses its function, we carried out similar fractionation analyses after treating leaves with the plant stress hormone ABA for 2 h. ABA is a negative regulator of H+-ATPase phosphorylation and activity (Haruta et al., 2015) and triggers stomatal closure (Thiel et al., 1993; Merlot et al., 2007; Jezek and Blatt, 2017; Xue et al., 2018).

Total cellular H+-ATPase density was considerably reduced in both wild-type and SYP132-OX leaves following ABA treatment. In wild-type leaves, ABA treatment reduced the H+-ATPase population in both plasma membrane and internal membrane compared with the control. In the SYP132-OX leaves, ABA treatment increased the plasma membrane-to-internal membrane ratio for H+-ATPase proteins compared with the control (Fig. 8, B, D, and F). These data indicated that ABA in wild-type plants promotes H+-ATPase traffic to reduce H+-ATPase density in both plasma and internal membranes. In SYP132-OX plants, where the population of the H+-ATPase proteins at the plasma membrane is already reduced, ABA drives reduction of the H+-ATPases in internal membranes.

In SYP132-OX leaves, following ABA treatment, the plasma membrane-to-internal membrane ratio for RFP-SYP132 was higher while the plasma membrane density of the fluorophore-fused SNARE was reduced when compared with the control, NAA, and fusicoccin treatments (Fig. 8, C, E, and G). These results suggested that ABA treatment reduces both plasma and internal membrane density of the RFP-SYP132.

Taken together, these data (Fig. 8; Supplemental Fig. S11) demonstrate that the hormones auxin and ABA affect the distribution of the H+-ATPase proteins at the plasma membrane. Likely, H+-ATPase traffic, in association with SYP132, dictates the availability of the H+-ATPase proteins at the plasma membrane for active function. A schematic model that consolidates our findings is shown in Figure 9.

DISCUSSION

The Qa-SNAREs SYP121 and SYP122 are most abundantly expressed throughout the plant and mediate bulk transport and secretion of cargo at the plasma membrane (Enami et al., 2009; Karnik et al., 2017; Waghmare et al., 2018). By contrast, the plasma membrane Qa-SNARE SYP132 is expressed in low abundance throughout the plant (Ichikawa et al., 2014). Nevertheless, SYP121 and SYP122 are not vital to the survival of plants. This is evident from the *syp121/syp122* double mutants, which are severely stunted in growth and yet are able to complete the growth cycle and produce seeds (Assaad et al., 2004). However, SYP132 is essential for plant viability, and the *syp132* mutant is embryo lethal (Enami et al., 2009; Ichikawa et al., 2014; Park et al., 2018). The studies outlined here identify SYP132 as a key player in H+-ATPase traffic at the plasma membrane that is moderated by plant hormones such as auxin. Along with our other observations of H+-ATPase function, this work demonstrates an unexpected role for SYP132 in the functional regulation of proton transport. Two key lines of evidence support these findings: (1) SYP132 expression is inversely related to H+-ATPase density at the plasma membrane; and (2) SYP132 expression is tissue specific and consistently affects plasma membrane H+-ATPase density and H+ extrusion to the apoplast as well as

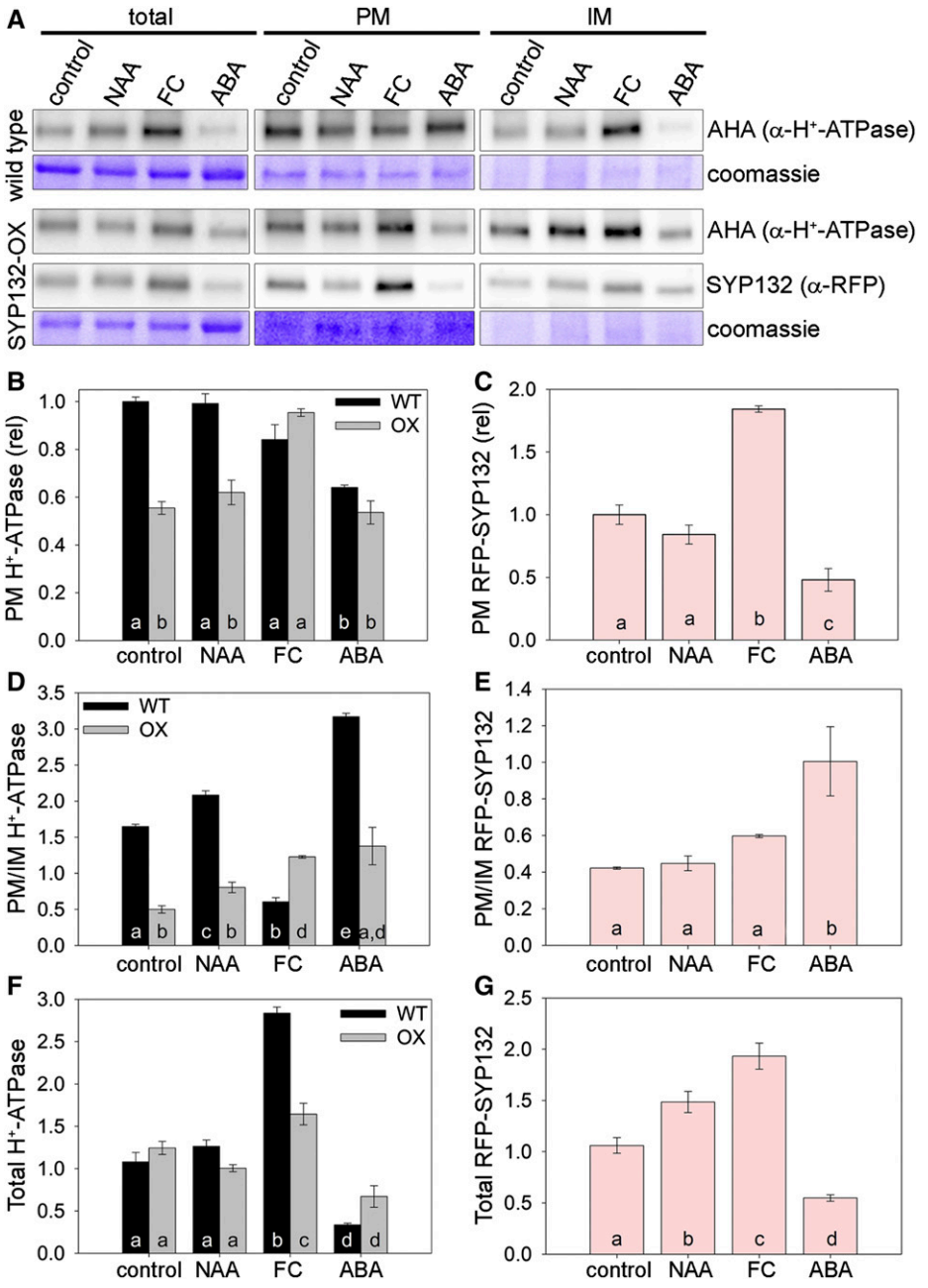

Figure 8. Plasma membrane H+-ATPase traffic is under the control of plant hormones and the fungal toxin fusicoccin (FC). A, Immunoblot analysis of leaf microsomal fractions (total), purified plasma membrane (PM), and internal membrane (IM) fractions of wild-type (top) and SYP132-OX (middle) Arabidopsis. Plasma membrane and internal membrane fractions were estimated to be ~95% pure (see Supplemental Fig. S11). Bands (AHA, ~95 kD; and RFP-SYP132, ~61 kD) were resolved on a single gel for immunoblot with anti-H+-ATPase and anti-RFP antibodies. Leaves were infiltrated with control (0.02% [v/v] ethanol in water), 10^{-5} M fusicoccin, 10^{-6} M NAA, and 10^{-5} M abscisic acid (ABA) for 2 h before fractionation of membranes by phase partitioning (see "Materials and Methods"). Total protein for each gel lane stained using Coomassie Blue stain (bottom) was used for quantitative analysis. B and C, Plasma membrane density relative to the wild-type control for H+-ATPase (B) and relative to the SYP132-OX control treatment for RFP-SYP132 (C). D and E, Ratio of plasma membrane to internal membrane density for H+-ATPase (D) and RFP-SYP132 (E). F and G, Total expression levels of the plasma membrane H+-ATPase relative to the wild-type control for H+-ATPase (F) and relative to the SYP132-OX control for RFP-SYP132 (G). All data represent means ± SE from three independent experiments. Statistical significance using ANOVA is indicated by letters ($P < 0.05$).

stomatal apertures and vegetative growth. Most importantly, our study identifies that the plant growth hormone auxin regulates *SYP132* expression; auxin-driven suppression of *SYP132* in growing shoots correlated with the auxin-induced increase in plasma membrane H+-ATPase density and function. While we have focused in part on AHA1 as a model H+-ATPase, we find that SYP132 affects H+-ATPase localization in each of the tissue types examined. Our findings thus suggest that SYP132 plays a critical role in promoting H+-ATPase internalization from the plasma membrane in both roots and shoots and is an important part of the mechanics of auxin-mediated control of pump activity at the plasma membrane.

H+-ATPase Traffic at the Plasma Membrane Unveiled by Dominant Negative SYP132

Qa-SNARE proteins are constituted of structural domains that are highly conserved across all eukaryotes and include a C-terminal transmembrane membrane anchor, a highly conserved H3 helix containing the SNARE motif vital for assembly of the SNARE core complex and regulatory Habc and N-terminal domains that fold back on the H3 helix to regulate cognate SNARE binding (Jahn and Scheller, 2006; Bassham and Blatt, 2008). All the domains of Qa-SNAREs contribute to the interactions essential for successful vesicle fusion events at the plasma membrane.

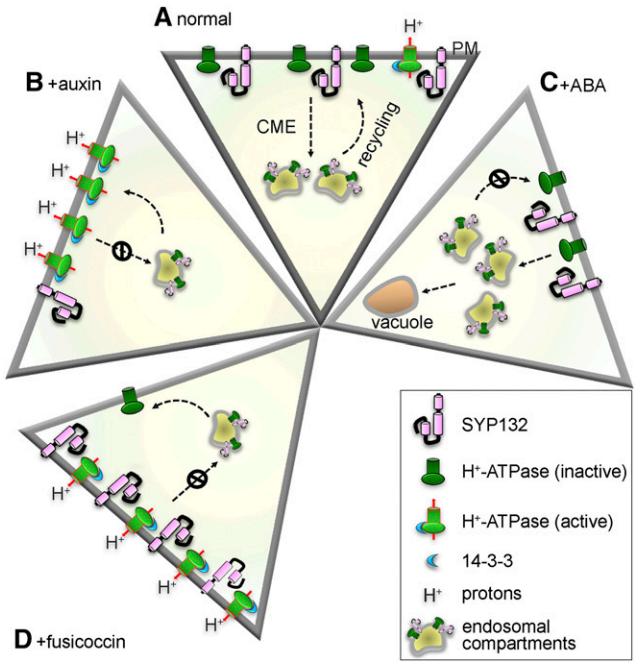

Figure 9. Model of SYP132-associated plasma membrane H+-ATPase traffic controlled by hormones. Net population of the H+-ATPase proteins at the plasma membrane reflects a balance of their exocytosis, endocytosis, and recycling. SYP132 affects H+-ATPase protein distribution between the plasma membrane and internal membrane compartments. A, H+-ATPase membrane traffic in normal growth conditions. CME of the H+-ATPase proteins from the plasma membrane in association with the low-abundance SYP132 is balanced by recycling and exocytotic delivery of the newly synthesized proteins (omitted for simplicity). The population of H+-ATPase proteins at the plasma membrane includes both inactive (dark green) and active (light green with red outline) pump proteins. B, The growth hormone auxin suppresses SYP132 expression, and consequently, SYP132-associated H+-ATPase traffic at the plasma membrane is reduced. Both density and activity of H+-ATPase proteins at the plasma membrane are augmented, allowing an increase in H+ extrusion into the apoplast due to auxin. C, The stress hormone ABA promotes SYP132-associated traffic of the H+-ATPases directed to the vacuole for degradation. Coopted with the H+-ATPases, the SYP132 protein density at the plasma membrane is reduced due to ABA, and H+ extrusion to apoplast is suppressed. D, The fungal toxin fusicoccin induces H+-ATPase activation by stabilizing the binding of H+-ATPase proteins with regulatory 14-3-3 proteins (blue crescent). Our hypothesis is that SYP132-associated endocytosis of the active H+-ATPase is blocked upon fusicoccin treatment and, consequently, the density of H+-ATPase and SYP132 proteins at the plasma membrane is augmented. In summary, H+-ATPase traffic from the plasma membrane is under the control of hormones and is unexpectedly co-opted with the secretory Qa-SNARE SYP132, affecting vegetative plant growth and morphogenesis. Dashed arrows indicate the direction of traffic to and from the plasma membrane, and circles with lines through the center indicate block of traffic.

Dominant negative strategies involving the overexpression of the Qa-SNARE fragments lacking one or more of these domains have been employed successfully over the past decades to disrupt SNARE function and to study Qa-SNARE-mediated secretory traffic (Kargul et al., 2001; Sutter et al., 2006; Tyrrell et al., 2007; Karnik et al., 2013; Grefen et al., 2015). Examples include the so-called Sp3 fragment SYP121$^{Habc\Delta}$, lacking the Qa-SNARE and C-terminal transmembrane domains essential for SNARE interactions (Kargul et al., 2001), and the so-called Sp2 fragments SYP121$^{\Delta C}$ and SYP122$^{\Delta C}$, lacking the C-terminal transmembrane domain required for targeted vesicle fusion at the plasma membrane (Sutter et al., 2006; Tyrrell et al., 2007). In this context, it is worth noting that Sutter et al. (2006) used overexpression of the SYP121 Sp2 fragment and observed a block of KAT1 K^+ channel traffic to the plasma membrane. The SYP121 Sp2 fragment blocks traffic mediated by both SYP121 and SYP122 (Tyrrell et al., 2007). They used the plasma membrane H+-ATPase as a control in these studies and reported that its cellular distribution was not affected by the SYP121 Sp2 fragment (Sutter et al., 2006). Thus, both SYP121 and SYP122 may be discounted for roles in H+-ATPase traffic at the plasma membrane.

A major drawback of the dominant negative Sp2 fragment approach is the overlaps in block of the traffic mediated by other Qa-SNAREs that share common cognate SNARE binding partners in a SNARE complex for secretion. When overexpressed, the Sp2 fragments are able to form SNARE complexes, but these complexes are not targeted to the plasma membrane for vesicle fusion, resulting in a block of secretory vesicle traffic at the plasma membrane (Tyrrell et al., 2007; Karnik et al., 2013, 2015, 2017). Although all three Qa-SNAREs SYP121, SYP122, and SYP132 bind to the same cognate SNARE partners (Karnik et al., 2013; Ichikawa et al., 2014), they mediate vesicle traffic of distinct cargoes (Kalde et al., 2007; Waghmare et al., 2018). Therefore, the use of dominant negative strategies that confer specificity in action are desirable. We discovered that the SYP132 SP3 fragment SYP132$^{Habc\Delta}$ blocked the secretion of SYP132-dependent secretory cargo, but its effect on the traffic of cargoes that rely on SYP132-independent pathways was much reduced (Supplemental Fig. S5). This specificity of SYP132$^{Habc\Delta}$ can be attributed to the soluble SYP132$^{Habc\Delta}$ peptides (Supplemental Fig. S3) that interact with the full-length SYP132 to inhibit its activity (Supplemental Fig. S4F). Additionally, the Qa-SNARE N terminus and Habc domains generally bind with regulatory proteins such as the SM (Sec1/Munc18-like) proteins (Südhof and Rothman, 2009; Karnik et al., 2013, 2015), which specifically regulate the Qa-SNARE function. For example, in Arabidopsis vegetative tissue, the SM protein SEC11 binds specifically with SYP121 to promote secretory traffic at the plasma membrane (Karnik et al., 2013), while the SM protein Sec1B is essential for SYP132-meditated secretory traffic to the plasma membrane (Karnahl et al., 2018). Hence, another possible explanation for SYP132$^{Habc\Delta}$ dominant negative action is that it may bind and titrate out the regulatory SM proteins essential for stabilized SNARE complex formation (Karnik et al., 2013), thereby suppressing SYP132-mediated secretory traffic at the plasma membrane.

In this study, the SYP132$^{Habc\Delta}$ fragment (Supplemental Fig. S4, A–E) was specifically used to block SYP132-mediated secretory traffic of the H$^+$-ATPases to the plasma membrane (Figs. 1 and 2). Logically, if SYP132 is involved in H$^+$-ATPase forward traffic, a block of SYP132-mediated secretion by the dominant negative SYP132$^{Habc\Delta}$ should perturb the delivery of the H$^+$-ATPases to the plasma membrane. Contrary to this supposition, SYP132$^{Habc\Delta}$ overexpression enhanced H$^+$-ATPase protein density at the plasma membrane (Figs. 1 and 2). These results suggest that SYP132 has an unexpected role in promoting the removal of H$^+$-ATPase proteins from the plasma membrane.

Plasma Membrane H$^+$-ATPase and SYP132 Endocytosis Is Coopted

The effects of the dominant negative SYP132$^{Habc\Delta}$ on H$^+$-ATPase traffic were supported by overexpression of the functional full-length SYP132, which promoted membrane traffic of the H$^+$-ATPase proteins from the plasma membrane to the internal membranes (Figs. 1–4; Supplemental Fig. S7), and they also lead to additional conclusions.

Qa-SNAREs that act as i-SNAREs are reported to form nonfusogenic complexes and block secretory traffic, contrary to their conventional roles in secretion (Varlamov et al., 2004). The reduction in density of the H$^+$-ATPase proteins at the plasma membrane in the SYP132-OX plants (Figs. 1–4; Supplemental Fig. S7) therefore could be attributed to the i-SNARE activity of SYP132, apparent upon the overexpression of the Qa-SNARE. However, the dominant negative SYP132$^{Habc\Delta}$, which logically must also block secretory traffic, instead augmented H$^+$-ATPase density at the plasma membrane (Figs. 1 and 2). Moreover, additional roles of SYP132 in promoting secretory traffic at the phragmoplast during cytokinesis are established (Park et al., 2018), rendering the possibility that it acts as an i-SNARE and interferes with secretory traffic unlikely.

Experiments with clathrin mutant Arabidopsis showed that SYP132-associated H$^+$-ATPase traffic was sensitive to clathrin (Fig. 3). Biochemical analysis of fractionated membranes (Fig. 4) showed that H$^+$-ATPase protein integration into the plasma membrane is inversely related to the levels of SYP132 expression (Supplemental Fig. S8). Indeed, the *syp132*^{T} mutant plants had almost double the H$^+$-ATPase density compared with the wild type, while the SYP132-OX plants had half as much H$^+$-ATPase density at the plasma membrane (Fig. 4; Supplemental Fig. S8). Taken together, these findings indicate an unusual role of the Qa-SNARE SYP132 in promoting H$^+$-ATPase residence in internal membranes relative to the plasma membrane.

SYP132 is primarily localized to the plasma membrane (Supplemental Fig. S4; Enami et al., 2009). Even so, SNARE-mediated vesicle traffic for secretion at the plasma membrane generally must occur in tandem with vesicle endocytosis for the regulation of vesicle membrane and cognate SNARE turnover (Karnik et al., 2013, 2015; Larson et al., 2017). Therefore, additional effects of SYP132 on post-synthesis H$^+$-ATPase delivery to the plasma membrane or on its recycling from endosomal compartments cannot be completely ruled out. Blocking H$^+$-ATPase forward traffic and Golgi retention following treatment with brefeldin A (BFA), an inhibitor of the Golgi apparatus, affects H$^+$ extrusion (Schindler et al., 1994; Lee et al., 2002), but SYP132 does not accumulate in BFA-sensitive compartments (Ichikawa et al., 2014). Thus, no compelling evidence exists for the role of SYP132 in BFA-sensitive forward traffic of the H$^+$-ATPase proteins. Interestingly, in the SYP132-OX leaves, the population of the RFP-SYP132 proteins localized to the internal membranes was higher compared with the plasma membrane (Figs. 1 and 4). Taken together, these finding suggest that traffic of the H$^+$-ATPases is tied with that of SYP132, and effectively this cooption of traffic allows for coordination between proton transport, secretory traffic, and vesicle membrane cycling.

SYP132 Affects the Physiology of Plant Growth and Stomatal Responses

The roles of SYP132-mediated traffic in plant physiology are substantiated by phenotypes corresponding to reduce plasma membrane H$^+$-ATPase activity; leaf apoplast pH was more alkaline in the SYP132-OX compared with the wild-type plants, and shoot growth was reduced (Fig. 5; Supplemental Fig. S9). In the SYP132-OX lines, reduced H$^+$-ATPase density at the plasma membrane (Fig. 4) corresponded to reduced proton pumping, an increase in pH of the apoplastic fluid, and a significant decrease in plant growth (Fig. 5; Supplemental Figs. S9 and S10). The pH of the apoplast is an important factor controlling the plasticity of the cell wall, and it varies rapidly and differentially between cell types during growth (Michelet and Boutry, 1995; Palmgren, 2001). These observations effectively highlight the roles of SYP132 in membrane traffic for the regulation of density of the plasma membrane H$^+$-ATPase proteins, which has direct consequences on the regulation of proton transport for plastic cell expansion.

In plants, stomata are excellent models to gauge H$^+$-ATPase function. Blue light-induced stomatal opening is mediated through activation of plasma membrane H$^+$-ATPases in guard cells (Yamauchi et al., 2016). Moreover, stomata must open and close in response to various environmental stimuli, including light, humidity, and foliar pathogens (Roelfsema and Hedrich, 2005; Shimazaki et al., 2007; Shope et al., 2008; Jezek and Blatt, 2017; Kaundal et al., 2017). Presumably, membrane traffic and function of primary transporters of guard cells, such as the plasma membrane H$^+$-ATPases and the KAT1 K$^+$ channels, must be tightly regulated in response to multiple environmental stimuli and stresses. The Qa-SNARE SYP121 mediates

recycling KAT1 K^+ channels to the plasma membrane for programmed stomatal closure and the regulation of stomatal opening (Sutter et al., 2006; Eisenach et al., 2012; Jezek and Blatt, 2017; Karnik et al., 2017). We found that the SYP132-OX lines showed smaller stomatal apertures compared with the wild type (Fig. 7), an observation that we attribute chiefly to reduced H^+-ATPase density and function at the plasma membrane. This semiclosed stomatal phenotype was reversed following treatment with the fungal toxin fusicoccin (Fig. 7), which activates the plasma membrane H^+-ATPase and the KAT1 K^+ channels by stabilizing their binding with the regulatory 14-3-3 proteins (Marre, 1979; Saponaro et al., 2017). These observations highlight the importance of the H^+-ATPase density and its regulation by SYP132 in guard cells, even if the Qa-SNARE has other roles in the regulation of stomatal responses.

Plasma Membrane H^+-ATPase Traffic Is Regulated by Plant Hormones

The most striking aspect of the SYP132-mediated membrane traffic is its hormone control. In growing shoot tissue, auxin further suppressed SYP132 transcript levels (Fig. 6) and, consequently, reduced the traffic of the H^+-ATPases from the plasma membrane to internal membrane compartments (Fig. 8D). A marked increase in plasma membrane H^+-ATPase density was noted in previous studies (Hager et al., 1991) and can be attributed to the block of endocytic traffic by the depletion of SYP132. The effect of SYP132 levels on H^+-ATPase traffic are the same in different plant tissues. Notably, differential regulation of SYP132 expression occurs in roots and shoots in the presence of high concentrations of auxin (Fig. 6). Thus, depending on hormonal cues, SYP132 expression and thereby H^+-ATPase density at the plasma membrane are modulated differentially.

The stress hormone ABA regulates plasma membrane H^+-ATPase activity, and in stomata, ABA drives closure to reduce water loss during drought (Merlot et al., 2007; Jezek and Blatt, 2017). Our data allow a new interpretation of recent data on ABA-mediated regulation of the H^+-ATPases. Recently, Xue et al. (2018) showed that ABA induces interactions between the plasma membrane H^+-ATPases and the R-SNARE VAMP711 for inhibition of proton pumping. However, VAMP711 is primarily localized at the tonoplast membrane (Heard et al., 2015) and it does not relocalize to the plasma membrane in response to ABA (Xue et al., 2018). This raises the possibility that ABA influences postendocytic traffic of the H^+-ATPase proteins. In our studies, the density of the H^+-ATPases at the plasma membrane was substantially reduced in wild-type plants in the presence of ABA, as in the SYP132-OX plants (Fig. 8, A and B). Total cellular H^+-ATPase and RFP-SYP132 levels were also reduced (Fig. 8, F and G). In light of these findings, we can place the hormone ABA as a promoter of H^+-ATPase endocytosis from the plasma membrane for degradation via the VAMP711 pathway to the vacuole.

An outstanding feature of SYP132-associated endocytic traffic is that it appears to be influenced by the functional status of the H^+-ATPase proteins (Figs. 7 and 8). ABA promotes H^+-ATPase dephosphorylation (MacRobbie, 1991; Meckel et al., 2004; Zhang et al., 2004) for inactivation of proton pumping. H^+-ATPase endocytosis is favored in the presence of ABA (Fig. 8). Conversely, fusicoccin locks the H^+-ATPase proteins in their active state (Marre, 1979; Saponaro et al., 2017), and in SYP132-OX plants, H^+-ATPase endocytosis from the plasma membrane was reduced following fusicoccin treatment (Figs. 7 and 8). Thus, for SYP132, we consider the possibility that hormonal regulation of membrane traffic associated with this Qa-SNARE coordinates with H^+-ATPase activity at various levels within the plant. Further research will help dissect the complexities of SYP132-associated traffic and its regulation during hormone cross talk.

CONCLUSION

In summary (see Fig. 9 for a model), we uncover a mechanism of cooption of the Qa-SNARE and the plasma membrane H^+-ATPase in vesicle traffic to maintain a steady turnover of H^+-ATPase proteins at the plasma membrane for active function. Traffic of active H^+-ATPase proteins at the plasma membrane is blocked to maintain proton extrusion, while inactivation of the H^+-ATPases promotes their removal from the plasma membrane. Thus, control of H^+-ATPase traffic is an important counterpart to its posttranslational regulation. We identify SYP132 and the endocytosis of the H^+-ATPases as novel and dominant elements of this regulation, which, in normal conditions, serves to maintain the functional pool of H^+-ATPases at the plasma membrane. Plant hormones, including auxin and ABA, govern SYP132-associated traffic in conjunction with their regulation of the H^+-ATPases for plant growth and morphogenesis. It will be of interest now to pursue these findings in relation to H^+-ATPase traffic in specialized tissues such as the growing pollen tubes (Certal et al., 2008), where these proteins are locally excluded from the growing tip. Interestingly, a proteomics screen for the Arabidopsis SYP132 interactome has identified the H^+-ATPase proteins as one of the SNARE binding partners (Fujiwara et al., 2014). Indeed, some interesting interactions of trafficking SNAREs with non-SNARE proteins are noted to affect cellular traffic and plant physiology (Honsbein et al., 2009; Faraco et al., 2017; Barozzi et al., 2019). We are currently investigating the dynamics of SYP132 interactions and their relationship to H^+-ATPase traffic as well as the physiology of plant growth. Our studies launch an exciting future research focus on the hormone regulation of membrane traffic for plant growth and morphogenesis.

MATERIALS AND METHODS

Plasmid Construction

Arabidopsis (*Arabidopsis thaliana*) SYP132, SYP132$^{Habc\Delta}$, and AHA1 were PCR amplified from complementary DNA and recombined using Gateway cloning (Invitrogen) to prepare entry clones in pDONR207, pDONR221-P1P4, or pDONR221-P3P2 vectors (Grefen and Blatt, 2012). Supplemental Table S2 lists all primers used for cloning in the study. The SYP121 entry clone was from previous work (Karnik et al., 2013; Zhang et al., 2015).

For balanced coexpression of proteins in plants, we used the Gateway-based 2in1 vector system, specifically the pFRET-2in1gc-NN vector (Hecker et al., 2015), to drive coexpression of GFP or mCherry fusion proteins, each under the control of the CaMV 35S promoter. For GFP-, RFP-, or YFP-fused SYP121, SYP132, SYP132$^{Habc\Delta}$, and AHA1 protein expression under the control of the CaMV 35S promoter in plants, constructs with Basta or kanamycin resistance for selection were cloned in Gateway-based vectors (Karimi et al., 2002).

Plant Growth and Transformation

Agrobacterium tumefaciens GV3101 carrying the desired constructs as described previously (Tyrrell et al., 2007) was used for all transient and stable plant transformations. Wild-type tobacco (*Nicotiana tabacum*) plants were grown in soil at 26°C and 70% relative humidity on a 16-h-day/8-h-night cycle. Four- to 6-week-old plants with three to four fully expanded leaves were selected for transient transformation of the leaf epidermis by infiltration with agrobacteria carrying the desired constructs as described previously (Karnik et al., 2013, 2015; Zhang et al., 2015). Transgenic stable lines of Arabidopsis ecotype Columbia-0 (wild type) expressing GFP- or RFP-fused SYP132 (SYP132-OX), YFP-SYP121 (SYP121-OX), and 35S:*GFP-AHA1* (AHA1-OX; Hashimoto-Sugimoto et al., 2013) coexpressing SYP132 (GFP-AHA1/RFP-SYP132) were generated by floral dip (Clough and Bent, 1998). As described previously (Karnik et al., 2015), three or more independent transformed lines were selected on 50 μg mL^{-1} Basta (phosphinothricin; Bayer Crop Science) or 50 μg mL^{-1} kanamycin (Harrison et al., 2006). Plants grown from T3 or T4 generation seeds of three independently transformed lines for each transgenic Arabidopsis line were analyzed in detail, and two lines, each showing similar fluorophore-fused protein expression in immunoblot analysis, were used for experiments. T-DNA insertion lines were analyzed by PCR genotyping to identify (http://signal.salk.edu/cgi-bin/tdnaexpress) heterozygous *syp132*^{T} (*At5g08080*; SAIL 403_B09) mutants as described (Park et al., 2018). Primers are listed in Supplemental Table S3.

Plant Treatments and Phenotype Analysis

Phenotypic analysis was carried out with each of the two independently transformed transgenic lines for GFP- and RFP-fused SYP132 (35S:GFP-SYP132: 1-1, 35S:GFP-SYP132: 3-1, 35S:RFP-SYP132: 1-1, and 35S:RFP-SYP132: 2-4). For simplicity, main figures show only RFP-SYP132: 2-4 as a representative.

Shoot Growth Analysis

Arabidopsis plants were grown in standard conditions on soil under an 8-h-light/16-h-dark, 18°C/22°C (light/dark) cycle with 150 μmol m^{-2} s^{-1} PAR light and 55% restricted humidity for biochemistry and stomatal aperture experiments. For shoot growth analysis, plants were grown on soil under a short-day 8-h-light/16-h-dark or a long-day 16-h-light/8-h-dark (light/dark) cycle for 3 weeks as described (Karnik et al., 2015).

Hypocotyl Elongation

Seeds were sterilized and placed on one-half-strength Murashige and Skoog (MS) medium (Sigma-Aldrich) containing 0.8% (w/v) agar and 0.5% (w/v) sucrose following stratification for 3 d at 4°C. Seed germination was activated by placing the plates under a red filter for 2 h and then allowing growth vertically in the dark for 4 d. Plates were scanned, and the length of the etiolated hypocotyls was measured using the Fiji (National Institutes of Health) software (Schindelin et al., 2012).

Apoplast Wash Fluid pH

Rosette leaves of 3-week-old Arabidopsis plants were infiltrated with water and immediately cut into 5- to 6-mm-wide strips. The strips were bundled, rolled, and loaded vertically (cut ends top and bottom) in microfuge spin columns; apoplast fluid was flushed out by centrifugation (3 min at 18,000 rpm; Grefen et al., 2015). Fluid from three different leaves from each plant was pooled, and pH was measured using a micro pH electrode.

Stomatal Aperture Measurements

Rosette leaves were obtained from 4-week-old plants grown on soil under an 8-h-light/16-h-dark, 18°C/22°C (light/dark) cycle with 150 μmol m^{-2} s^{-1} PAR light and 55% restricted humidity. Intact leaf stomatal pores were stained with propidium iodide for imaging to measure stomatal aperture as described (Chitrakar and Melotto, 2010). Treatments were with control (0.02% [v/v] ethanol in water), with 10 μM fusicoccin (Hashimoto-Sugimoto et al., 2013), or with 5 μM ABA (Merlot et al., 2007), for 2 h.

Samples for Imaging

Imaging of transiently transformed tobacco plants was carried out 2 d following transformation using leaf sections infiltrated with water or with 1 M NaCl for plasmolysis.

Three-day-old wild-type or 35S:GFP-AHA1 Arabidopsis seedlings grown in sterile liquid one-half-strength MS medium were transiently transformed with *A. tumefaciens* as described previously (Grefen et al., 2010). Imaging of root hairs was carried out 2 d following the transformation of seedlings.

Genotyping and RT-qPCR Analysis

Plant Growth and Sample Preparation

Surface-sterilized Arabidopsis seeds were vernalized for 2 to 3 d at 4°C. Seedlings were grown vertically at 22°C and 150 μmol m^{-2} s^{-1} under a 16-h-light/8-h-dark cycle on one-half-strength MS medium supplemented with 0.5% (w/v) Suc and 0.8% (w/v) agar. Five to 7 d after germination, seedling shoots and roots were separated by cutting with a scalpel and incubated separately in liquid one-half-strength MS medium or one-half-strength MS medium supplemented with 10^{-6} M NAA for 60 and 180 min. Approximately 100 roots per sample were collected by flash freezing in liquid N_2.

RNA Isolation and RT-qPCR

Total RNA was extracted and purified by the TRIzoI Plus RNA purification kit (Invitrogen) as per the supplier's manual. One microgram of total RNA from each sample was used for the synthesis of complementary DNA using the Quanti Tect Reverse Transcription Kit (Qiagen). RT-qPCR was performed with Brilliant III Ultra-Fast SYBR Green qPCR Master Mix (Agilent) as per the manufacturer's recommendation in the Step One Plus Real-Time PCR System (Thermo Fisher). The gene-specific primer pairs are listed in Supplemental Table S4. Relative gene expression was calculated ($2^{-\Delta CT}$ method) with the mitochondrial 18S rRNA (*AtMg01390*) as the reference gene. Fold change in gene expression following NAA was calculated as $2^{-\Delta\Delta CT}$ (Livak and Schmittgen, 2001). Primers, as described (Enami et al., 2009), are listed in Supplemental Table S4.

Confocal Imaging

Confocal images of tobacco epidermis and Arabidopsis root hair were collected using a Leica TCS SP8-SMD confocal microscope with spectral GaAsP detectors. Images were collected using 40×/0.75NA and 63×/0.75NA oil-immersion objective lenses, respectively. For secretory traffic assay, images were acquired from tobacco epidermis using the 20×/0.75NA air objective. GFP fluorescence was excited with continuous 488 nm or 20 MHz-pulsed 470-nm light and collected over 500 to 535 nm. mCherry fluorescence was collected over 590 to 645 nm following excitation at 552 nm. RFP was excited with 552-nm light, and RFP fluorescence emission was collected over 560 to 615 nm. FM4-64 was excited using the 488-nm laser line, and emission was collected over 750 to 780 nm. For stomatal aperture measurements, imaging of the lower surface of the leaves was carried out as described (Chitrakar and Melotto, 2010) using a 20×/0.75 NA air objective lens to detect the fluorescence of propidium iodide by excitation at 453 nm and emission at 543 to 620 nm.

Quantification of Fluorescence Distribution

Cell Peripheral-Internal Fluorescence Distribution

To quantify the distribution of the fluorophore-fused proteins between the cell periphery and its interior, transiently transformed tobacco epidermis cells were plasmolyzed with 1 M NaCl to retract the plasma membrane and resolve the cell interior. Confocal images were collected as Z-stacks and rendered as 3D projections (Supplemental Fig. S1) prior to analysis. For each cell, ROIs demarcating cell periphery (width of ~1.5 μm) and cell interior were traced using the bright-field image overlay as reference. Integrated fluorescence density was measured using Fiji (National Institutes of Health) software for each ROI and corrected for background fluorescence using the equation [corrected total fluorescence = integrated density – (area of selected ROI × mean fluorescence of background)], as described (Marwaha and Sharma, 2017). The proportion of fluorophore distribution at the cell periphery and interior was represented as bar graphs of mean peripheral-internal fluorescence ratios.

Fluorescence Distribution in the Cell Interior

To quantify the proportion of internalization in root hair cells, an outline was drawn to define the cell interior using the rectangular selection tool and the bright-field image for reference. Also, the region of the cell periphery was defined by tracing an ~1.5-μm-wide line using the bright-field image as a reference. Mean fluorescence was measured for each region and ratioed as internal-periphery, as a measure of internalization, which was plotted as bar graphs and accounted for the expression levels for each fluorophore in the cells.

Fluorescence Distribution at the Cell Periphery for Puncta

To quantify the proportion of fluorophore-tagged protein distributed to puncta, percentage relative SD analysis was used as described (Eisenach et al., 2014). Briefly, the percentage relative SD of intensities determined from a one-pixel-wide line around the periphery of plasmolyzed cells using the bright-field image as reference was measured using Fiji (National Institutes of Health) and normalized to the intensity means.

Membrane Fractionation Two-Phase System

Microsomal membrane isolation and aqueous two-phase partitioning were conducted based on modified procedures (Yoshida et al., 1983; Advani et al., 1999; Alexandersson et al., 2008; Yang and Murphy, 2013). Briefly, freshly harvested 4-week-old Arabidopsis rosettes were ground with mortar and pestle in homogenization buffer (330 mM Suc, 25 mM HEPES-KOH, pH 7.5, 5 mM EDTA-KOH, 0.2% [w/v] BSA, 0.6% [w/v] polyvinylpyrrolidone [PVP40; Sigma-Aldrich], 5 mM dithiothreitol [DTT], 5 mM ascorbic acid, 0.5 mM phenylmethylsulfonyl fluoride, and protease inhibitor [Thermo Fisher Scientific]). The homogenates were filtered through Miracloth (Merck) and then centrifuged at 8,000*g* at 4°C for 15 min. Microsomal pellets were collected by centrifugation of supernatants at 100,000*g* at 4°C for 1 h and resuspended with resuspension buffer (buffer R: 330 mM Suc, 5 mM potassium phosphate [a mixture of 200 mM KH_2PO_4 and 200 mM K_2HPO_4, pH 7.8], 0.1 mM EDTA-KOH, 0.1 mM EGTA, 1 mM DTT, protease inhibitor cocktail, and 100 mM phenylmethylsulfonyl fluoride). Resuspended microsomal membranes were added to a 27g phase buffer (6.5% [w/v] Dextran T500, 6.5% [w/v] PEG3350, 330 mM Suc, 5 mM potassium phosphate, and 3 mM KCl), and phases were collected separately at 1,500*g* at 4°C for 15 min. Upper and lower phases were repartitioned twice with fresh lower or upper phase (without membranes). Purified phases were diluted with buffer R 3-fold for upper phases and 10-fold for lower phases. Plasma (upper) and internal (lower) membranes were collected by centrifugation at 100,000*g* and 4°C for 1 h and resuspended in buffer R. Protein quantity was determined using Bradford (Bio-Rad) with BSA Fraction V as a standard.

Immunoblot

Sample Preparation

Plant samples for immunoblot were prepared as described (Karnik et al., 2015). Briefly, plant leaves were excised and flash frozen in liquid N_2. Frozen tissue was ground in equal volumes (w/v) of homogenization buffer containing 500 mM Suc, 10% (w/v) glycerol, 20 mM EDTA, 20 mM EGTA, protease inhibitor (Roche), 10 mM ascorbic acid, 5 mM DTT, and 50 mM Tris-HCl, pH 7.4, and centrifuged at 13,000*g* and 4°C for 30 min to pellet debris. Supernatant was diluted to 10 $\mu g\ \mu L^{-1}$ in homogenization buffer and mixed 1:1 with Laemmli buffer containing 2.5% (v/v) 2-mercaptoethanol, heated to 95°C for 10 min, and separated by SDS-PAGE. Proteins from yeast were prepared as described previously (Grefen et al., 2010). All samples were diluted in loading buffer to 5 mg protein mL^{-1} per lane. Ponceau S-stained Rubisco bands were used as loading standards for plant samples.

Immunoblot

Nitrocellulose membranes with transferred separated proteins were first probed with primary antibodies: anti-GFP (1:5,000 dilution; Abcam), anti-mCherry (1:5,000 dilution; Abcam), anti-H+-ATPase (1:2,500 dilution; Agrisera), anti-KAT1 (1:500 dilution; Agrisera), anti-BiP (lumen-binding protein; 1:2,500 dilution; Agrisera), and anti-YFP (1:3,000 dilution; Agrisera). Subsequently, secondary antibody goat anti-rabbit-horseradish peroxidase conjugate (1:20,000 dilution; Abcam) was used. Cross-reacting bands were visualized using West Femto Super Signal chemiluminescence detection (Thermo Pierce) and imaged by Fusion Chemiluminescence imager (Peqlab). In the two-phase experiments, membranes were cut in the middle to probe with separate sets of antibodies on the same membrane for the detection of proteins with significant differences in M_r. In some experiments, membranes were reprobed after stripping in 100 mM β-mercaptoethanol, 2% (w/v) SDS, and 62.5 mM Tris-HCl, pH 6.7, at 50°C for 15 min. For comparative analysis of immunoblot band density, densitometry data were normalized against corresponding total protein density for each gel lane by Coomassie Blue stain.

Immunoblot Analysis

Immunoblot band intensities in each lane for different proteins were measured using the Fiji (National Institutes of Health) gel analysis plug-in and normalized against the intensity of corresponding loading controls. Mean band intensity data were calculated and statistically analyzed from $n = 3$ experiments and plotted as a measure of protein density.

Yeast GPS System

Protein-protein interactions were done for SYP132$^{\Delta C}$ and SYP132 $^{Habc\Delta}$ as baits in vector pEXG2Met-Dest and for SYP132, VAMP721, and SNAP33 as prey in vector pNX35-Dest (Grefen et al., 2009). The yeast GPS assay was performed as described (Zhang et al., 2018). The bait constructs were transferred in yeast strain THY.AP4, and prey constructs were transferred in THY.AP5. Ten to 15 yeast colonies were selected and inoculated into selective medium (CSM_{LM} for THY.AP4 and CSM_{-TUM} for THY.AP5) for overnight growth at 180 rpm and 28°C. Liquid cultures were harvested and resuspended in Yeast extract- Peptone-Dextrose (YPD) medium. Yeast mating was performed in sterile PCR tubes by mixing equal aliquots of yeast containing bait and prey construct. Aliquots of 5 μL were dropped on YPD plates and incubated at 28°C overnight. Then, colonies were transferred from YPD plates onto CSM_{LTUM} plates and incubated at 28°C for 2 to 3 d. Diploid colonies were selected and inoculated in liquid CSM_{-LTUM} medium and grown at 180 rpm 28°C overnight. Then, the yeast was harvested and resuspended in sterile water. Serial dilutions at OD_{600} of 1 and 0.1 in water were dropped on CSM_{AHLTUM} plates (5 μL per spot), with Met added at increasing concentrations. Plates were incubated at 28°C, and images were taken after 3 d. Yeast were also dropped on CSM_{-LTUM} control plates to confirm mating efficiency and cell density, and growth was imaged after 24 h at 28°C. To verify expression, yeast was harvested and extracted for protein gel-blot analysis using anti-HA antibody (Roche) for prey and anti-VP16 antibody (Abcam) for bait.

Statistical Analysis

Data are means ± SE of $n \geq 3$. Statistical analysis was performed using Sigmaplot 11.2 (Systat Software). Significance was determined by Student's *t* test or ANOVA using the Holm-Sidak method for all pairwise multiple comparisons, $P < 0.05$.

Materials and Correspondence

35S:*GFP*-AHA1 seeds (Hashimoto-Sugimoto et al., 2013) were a kind gift from the Koh Iba lab. Clathrin mutant CHC1 and HUB1 seeds (Larson et al.,

2017), the 2in1 and plant expression plasmids (Karnik et al., 2015), entry clones for KAT1 and SYP121, and all constructs for the secretory traffic assay (Waghmare et al., 2018) were gifts from the Mike Blatt lab.

Data Availability

Vectors are available at www.psrg.org.uk.

Accession Numbers

Transgenic lines used in the study are as follows: for CHC1 (At3g11130) T-DNA mutants, *chc1-1* (SALK_112213) and *chc1-2* (SALK_103252); for the SYP132 T-DNA mutant (*syp132*^{T}), SAIL_403_B09. Sequence data from this work can be found in the Arabidopsis Genome Initiative or GenBank/EMBL databases under the following accession numbers: AHA1 (*At2g18960*), SYP121 (*At3g11820*), SYP123 (*At4g03330*), SYP132 (full length; *At5g08080.1*), SYP132$^{Habc\Delta}$ (*At5g08080.2*), VAMP721 (*At1g04750*), SNAP33 (*At5g61210*), SBT5.2 (*At4g30270*), MERI5 (*At1g20160*), and KAT1 (*At5g46240*).

Supplemental Data

The following supplemental materials are available.

Supplemental Figure S1. SYP132 affects AHA1 distribution in tobacco epidermal cells.

Supplemental Figure S2. Immunoblots for transient transformations to verify protein expression.

Supplemental Figure S3. Qa-SNARE localization at the plasma membrane.

Supplemental Figure S4. Domian organization of dominant negative SYP132$^{Habc\Delta}$ and its interactions with cognate SNAREs.

Supplemental Figure S5. Dominant negative SYP132$^{Habc\Delta}$ affects SYP132-dependent secretory traffic at the plasma membrane.

Supplemental Figure S6. SYP132 does not affect the distribution of KAT1 puncta.

Supplemental Figure S7. Stable SYP132 overexpression affects AHA1 internalization.

Supplemental Figure S8. SYP132 protein and mRNA transcript expression in transgenic overexpression and mutant Arabidopsis lines.

Supplemental Figure S9. Independently transformed transgenic SYP132-OX Arabidopsis lines have similar phenotypes.

Supplemental Figure S10. Increased AHA1 density at the plasma membrane promotes shoot growth.

Supplemental Figure S11. Immunoblots of membrane fractions following treatment with plant hormones and fungal toxin fusicoccin.

Supplemental Table S1. Binding efficiency of primers used in RT-qPCR.

Supplemental Table S2. Primers used in molecular cloning.

Supplemental Table S3. List of primers used for genotyping.

Supplemental Table S4. List of primers used for RT-qPCR.

ACKNOWLEDGMENTS

We thank Mike Blatt for critical reading of the article and Amparo Ruiz-Prado for help with the logistics of plant propagation.

Received March 5, 2019; accepted March 22, 2019; published March 29, 2019.

LITERATURE CITED

Advani RJ, Yang B, Prekeris R, Lee KC, Klumperman J, Scheller RH (1999) VAMP-7 mediates vesicular transport from endosomes to lysosomes. J Cell Biol **146:** 765–776

Alexandersson E, Gustavsson N, Bernfur K, Karlsson A, Kjellbom P, Larsson C (2008) Purification and proteomic analysis of plant plasma membranes. Methods Mol Biol **432:** 161–173

Arango M, Gévaudant F, Oufattole M, Boutry M (2003) The plasma membrane proton pump ATPase: The significance of gene subfamilies. Planta **216:** 355–365

Assaad FF, Qiu JL, Youngs H, Ehrhardt D, Zimmerli L, Kalde M, Wanner G, Peck SC, Edwards H, Ramonell K, et al (2004) The PEN1 syntaxin defines a novel cellular compartment upon fungal attack and is required for the timely assembly of papillae. Mol Biol Cell **15:** 5118–5129

Barozzi F, Papadia P, Stefano G, Renna L, Brandizzi F, Migoni D, Fanizzi FP, Piro G, Di Sansebastiano GP (2019) Variation in membrane trafficking linked to SNARE AtSYP51 interaction with aquaporin NIP1;1. Front Plant Sci **9:** 1949

Bassham DC, Blatt MR (2008) SNAREs: Cogs and coordinators in signaling and development. Plant Physiol **147:** 1504–1515

Bock JB, Matern HT, Peden AA, Scheller RH (2001) A genomic perspective on membrane compartment organization. Nature **409:** 839–841

Catalano CM, Czymmek KJ, Gann JG, Sherrier DJ (2007) Medicago truncatula syntaxin SYP132 defines the symbiosome membrane and infection droplet membrane in root nodules. Planta **225:** 541–550

Certal AC, Almeida RB, Carvalho LM, Wong E, Moreno N, Michard E, Carneiro J, Rodriguéz-Léon J, Wu HM, Cheung AY, et al (2008) Exclusion of a proton ATPase from the apical membrane is associated with cell polarity and tip growth in *Nicotiana tabacum* pollen tubes. Plant Cell **20:** 614–634

Chitrakar R, Melotto M (2010) Assessing stomatal response to live bacterial cells using whole leaf imaging. J Vis Exp **44:** e2185

Clough SJ, Bent AF (1998) Floral dip: A simplified method for Agrobacterium-mediated transformation of Arabidopsis thaliana. Plant J **16:** 735–743

Cosgrove DJ (1987) Wall relaxation and the driving forces for cell expansive growth. Plant Physiol **84:** 561–564

Dhonukshe P, Aniento F, Hwang I, Robinson DG, Mravec J, Stierhof YD, Friml J (2007) Clathrin-mediated constitutive endocytosis of PIN auxin efflux carriers in Arabidopsis. Curr Biol **17:** 520–527

Di Sansebastiano GP, Barozzi F, Piro G, Denecke J, de Marcos Lousa C (2017) Trafficking routes to the plant vacuole: Connecting alternative and classical pathways. J Exp Bot **69:** 79–90

Eisenach C, Chen ZH, Grefen C, Blatt MR (2012) The trafficking protein SYP121 of Arabidopsis connects programmed stomatal closure and K^+ channel activity with vegetative growth. Plant J **69:** 241–251

Eisenach C, Papanatsiou M, Hillert EK, Blatt MR (2014) Clustering of the K^+ channel GORK of Arabidopsis parallels its gating by extracellular K^+. Plant J **78:** 203–214

El Kasmi F, Krause C, Hiller U, Stierhof YD, Mayer U, Conner L, Kong L, Reichardt I, Sanderfoot AA, Jürgens G (2013) SNARE complexes of different composition jointly mediate membrane fusion in Arabidopsis cytokinesis. Mol Biol Cell **24:** 1593–1601

Enami K, Ichikawa M, Uemura T, Kutsuna N, Hasezawa S, Nakagawa T, Nakano A, Sato MH (2009) Differential expression control and polarized distribution of plasma membrane-resident SYP1 SNAREs in Arabidopsis thaliana. Plant Cell Physiol **50:** 280–289

Evans ML, Ishikawa H, Estelle MA (1994) Responses of Arabidopsis roots to auxin studied with high temporal resolution: Comparison of wild-type and auxin-response mutants. Planta **194:** 215–222

Faraco M, Li Y, Li S, Spelt C, Di Sansebastiano GP, Reale L, Ferranti F, Verweij W, Koes R, Quattrocchio FM (2017) A tonoplast P_{3B}-ATPase mediates fusion of two types of vacuoles in petal cells. Cell Rep **19:** 2413–2422

Fasshauer D, Eliason WK, Brünger AT, Jahn R (1998) Identification of a minimal core of the synaptic SNARE complex sufficient for reversible assembly and disassembly. Biochemistry **37:** 10354–10362

Fendrych M, Leung J, Friml J (2016) TIR1/AFB-Aux/IAA auxin perception mediates rapid cell wall acidification and growth of Arabidopsis hypocotyls. eLife **5:** e19048

Foresti O, daSilva LLP, Denecke J (2006) Overexpression of the Arabidopsis syntaxin PEP12/SYP21 inhibits transport from the prevacuolar compartment to the lytic vacuole in vivo. Plant Cell **18:** 2275–2293

Fuglsang AT, Borch J, Bych K, Jahn TP, Roepstorff P, Palmgren MG (2003) The binding site for regulatory 14-3-3 protein in plant plasma membrane H^+-ATPase: Involvement of a region promoting phosphorylation-independent interaction in addition to the

phosphorylation-dependent C-terminal end. J Biol Chem **278:** 42266–42272

Fujiwara M, Uemura T, Ebine K, Nishimori Y, Ueda T, Nakano A, Sato MH, Fukao Y (2014) Interactomics of Qa-SNARE in Arabidopsis thaliana. Plant Cell Physiol **55:** 781–789

Gaffield MA, Betz WJ (2006) Imaging synaptic vesicle exocytosis and endocytosis with FM dyes. Nat Protoc **1:** 2916–2921

Geelen D, Leyman B, Batoko H, Di Sansebastiano GP, Moore I, Blatt MR (2002) The abscisic acid-related SNARE homolog NtSyr1 contributes to secretion and growth: Evidence from competition with its cytosolic domain. Plant Cell **14:** 387–406

Geldner N, Anders N, Wolters H, Keicher J, Kornberger W, Muller P, Delbarre A, Ueda T, Nakano A, Jürgens G (2003) The Arabidopsis GNOM ARF-GEF mediates endosomal recycling, auxin transport, and auxin-dependent plant growth. Cell **112:** 219–230

Grefen C, Blatt MR (2012) A 2in1 cloning system enables ratiometric bimolecular fluorescence complementation (rBiFC). Biotechniques **53:** 311–314

Grefen C, Obrdlik P, Harter K (2009) The determination of protein-protein interactions by the mating-based split-ubiquitin system (mbSUS). Methods Mol Biol **479:** 217–233

Grefen C, Donald N, Hashimoto K, Kudla J, Schumacher K, Blatt MR (2010) A ubiquitin-10 promoter-based vector set for fluorescent protein tagging facilitates temporal stability and native protein distribution in transient and stable expression studies. Plant J **64:** 355–365

Grefen C, Karnik R, Larson E, Lefoulon C, Wang Y, Waghmare S, Zhang B, Hills A, Blatt MR (2015) A vesicle-trafficking protein commandeers Kv channel voltage sensors for voltage-dependent secretion. Nat Plants **1:** 15108

Hager A (2003) Role of the plasma membrane H+-ATPase in auxin-induced elongation growth: Historical and new aspects. J Plant Res **116:** 483–505

Hager A, Menzel H, Krauss A (1971) Experiments and hypothesis concerning the primary action of auxin in elongation growth. Planta **100:** 47–75

Hager A, Debus G, Edel HG, Stransky H, Serrano R (1991) Auxin induces exocytosis and the rapid synthesis of a high-turnover pool of plasma-membrane H+-ATPase. Planta **185:** 527–537

Harper JF, Surowy TK, Sussman MR (1989) Molecular cloning and sequence of cDNA encoding the plasma membrane proton pump (H+-ATPase) of Arabidopsis thaliana. Proc Natl Acad Sci USA **86:** 1234–1238

Harrison SJ, Mott EK, Parsley K, Aspinall S, Gray JC, Cottage A (2006) A rapid and robust method of identifying transformed Arabidopsis thaliana seedlings following floral dip transformation. Plant Methods **2:** 19

Haruta M, Sussman MR (2012) The effect of a genetically reduced plasma membrane protonmotive force on vegetative growth of Arabidopsis. Plant Physiol **158:** 1158–1171

Haruta M, Burch HL, Nelson RB, Barrett-Wilt G, Kline KG, Mohsin SB, Young JC, Otegui MS, Sussman MR (2010) Molecular characterization of mutant Arabidopsis plants with reduced plasma membrane proton pump activity. J Biol Chem **285:** 17918–17929

Haruta M, Gray WM, Sussman MR (2015) Regulation of the plasma membrane proton pump (H+-ATPase) by phosphorylation. Curr Opin Plant Biol **28:** 68–75

Hashimoto-Sugimoto M, Higaki T, Yaeno T, Nagami A, Irie M, Fujimi M, Miyamoto M, Akita K, Negi J, Shirasu K, et al (2013) A Munc13-like protein in Arabidopsis mediates H+-ATPase translocation that is essential for stomatal responses. Nat Commun **4:** 2215

Heard W, Sklenář J, Tomé DFA, Robatzek S, Jones AME (2015) Identification of regulatory and cargo proteins of endosomal and secretory pathways in Arabidopsis thaliana by proteomic dissection. Mol Cell Proteomics **14:** 1796–1813

Hecker A, Wallmeroth N, Peter S, Blatt MR, Harter K, Grefen C (2015) Binary 2in1 vectors improve in planta (co)localization and dynamic protein interaction studies. Plant Physiol **168:** 776–787

Higaki T, Hashimoto-Sugimoto M, Akita K, Iba K, Hasezawa S (2014) Dynamics and environmental responses of PATROL1 in Arabidopsis subsidiary cells. Plant Cell Physiol **55:** 773–780

Honsbein A, Sokolovski S, Grefen C, Campanoni P, Pratelli R, Paneque M, Chen Z, Johansson I, Blatt MR (2009) A tripartite SNARE-K+ channel complex mediates in channel-dependent K+ nutrition in Arabidopsis. Plant Cell **21:** 2859–2877

Huisman R, Hontelez J, Mysore KS, Wen J, Bisseling T, Limpens E (2016) A symbiosis-dedicated SYNTAXIN OF PLANTS 13II isoform controls the formation of a stable host-microbe interface in symbiosis. New Phytol **211:** 1338–1351

Ichikawa M, Hirano T, Enami K, Fuselier T, Kato N, Kwon C, Voigt B, Schulze-Lefert P, Baluška F, Sato MH (2014) Syntaxin of plant proteins SYP123 and SYP132 mediate root hair tip growth in Arabidopsis thaliana. Plant Cell Physiol **55:** 790–800

Jahn R, Scheller RH (2006) SNAREs: Engines for membrane fusion. Nat Rev Mol Cell Biol **7:** 631–643

Jezek M, Blatt MR (2017) The membrane transport system of the guard cell and its integration for stomatal dynamics. Plant Physiol **174:** 487–519

Kalde M, Nühse TS, Findlay K, Peck SC (2007) The syntaxin SYP132 contributes to plant resistance against bacteria and secretion of pathogenesis-related protein 1. Proc Natl Acad Sci USA **104:** 11850–11855

Kargul J, Gansel X, Tyrrell M, Sticher L, Blatt MR (2001) Protein-binding partners of the tobacco syntaxin NtSyr1. FEBS Lett **508:** 253–258

Karimi M, Inzé D, Depicker A (2002) GATEWAY vectors for Agrobacterium-mediated plant transformation. Trends Plant Sci **7:** 193–195

Karnahl M, Park M, Krause C, Hiller U, Mayer U, Stierhof YD, Jürgens G (2018) Functional diversification of *Arabidopsis* SEC1-related SM proteins in cytokinetic and secretory membrane fusion. Proc Natl Acad Sci USA **115:** 6309–6314

Karnik R, Grefen C, Bayne R, Honsbein A, Köhler T, Kioumourtzoglou D, Williams M, Bryant NJ, Blatt MR (2013) Arabidopsis Sec1/Munc18 protein SEC11 is a competitive and dynamic modulator of SNARE binding and SYP121-dependent vesicle traffic. Plant Cell **25:** 1368–1382

Karnik R, Zhang B, Waghmare S, Aderhold C, Grefen C, Blatt MR (2015) Binding of SEC11 indicates its role in SNARE recycling after vesicle fusion and identifies two pathways for vesicular traffic to the plasma membrane. Plant Cell **27:** 675–694

Karnik R, Waghmare S, Zhang B, Larson E, Lefoulon C, Gonzalez W, Blatt MR (2017) Commandeering channel voltage sensors for secretion, cell turgor, and volume control. Trends Plant Sci **22:** 81–95

Kaundal A, Ramu VS, Oh S, Lee S, Pant B, Lee HK, Rojas CM, Senthil-Kumar M, Mysore KS (2017) GENERAL CONTROL NONREPRESSIBLE4 degrades 14-3-3 and the RIN4 complex to regulate stomatal aperture with implications on nonhost disease resistance and drought tolerance. Plant Cell **29:** 2233–2248

Kinoshita T, Shimazaki Ki (1999) Blue light activates the plasma membrane H+-ATPase by phosphorylation of the C-terminus in stomatal guard cells. EMBO J **18:** 5548–5558

Kitakura S, Vanneste S, Robert S, Löfke C, Teichmann T, Tanaka H, Friml J (2011) Clathrin mediates endocytosis and polar distribution of PIN auxin transporters in Arabidopsis. Plant Cell **23:** 1920–1931

Larson ER, Van Zelm E, Roux C, Marion-Poll A, Blatt MR (2017) Clathrin heavy chain subunits coordinate endo- and exocytic traffic and affect stomatal movement. Plant Physiol **175:** 708–720

Lee MH, Min MK, Lee YJ, Jin JB, Shin DH, Kim DH, Lee KH, Hwang I (2002) ADP-ribosylation factor 1 of Arabidopsis plays a critical role in intracellular trafficking and maintenance of endoplasmic reticulum morphology in Arabidopsis. Plant Physiol **129:** 1507–1520

Limpens E, Ivanov S, van Esse W, Voets G, Fedorova E, Bisseling T (2009) Medicago N_2-fixing symbiosomes acquire the endocytic identity marker Rab7 but delay the acquisition of vacuolar identity. Plant Cell **21:** 2811–2828

Livak KJ, Schmittgen TD (2001) Analysis of relative gene expression data using real-time quantitative PCR and the 2(-Delta Delta C(T)) method. Methods **25:** 402–408

MacRobbie EAC (1991) Effect of ABA on ion transport and stomatal regulation. *In* WJ Davies, HG Jones, eds, Abscisic Acid: Physiology and Biochemistry. Bios Scientific, Oxford, UK, pp 153–168

Marre E (1979) Fusicoccin: Tool in plant physiology. Annu Rev Plant Physiol Plant Mol Biol **30:** 273–288

Marwaha R, Sharma M (2017) DQ-Red BSA trafficking assay in cultured cells to assess cargo delivery to lysosomes. Bio Protoc **7:** e2571

Meckel T, Hurst AC, Thiel G, Homann U (2004) Endocytosis against high turgor: Intact guard cells of Vicia faba constitutively endocytose fluorescently labelled plasma membrane and GFP-tagged K-channel KAT1. Plant J **39:** 182–193

Merlot S, Leonhardt N, Fenzi F, Valon C, Costa M, Piette L, Vavasseur A, Genty B, Boivin K, Müller A, et al (2007) Constitutive activation of a

plasma membrane H^+-ATPase prevents abscisic acid-mediated stomatal closure. EMBO J **26:** 3216–3226

Michelet B, Boutry M (1995) The plasma membrane H^+-ATPase: A highly regulated enzyme with multiple physiological functions. Plant Physiol **108:** 1–6

Omelyanchuk NA, Wiebe DS, Novikova DD, Levitsky VG, Klimova N, Gorelova V, Weinholdt C, Vasiliev GV, Zemlyanskaya EV, Kolchanov NA, et al (2017) Auxin regulates functional gene groups in a fold-change-specific manner in Arabidopsis thaliana roots. Sci Rep **7:** 2489

Palmgren MG (2001) Plant plasma membrane H^+-ATPases: Powerhouses for nutrient uptake. Annu Rev Plant Physiol Plant Mol Biol **52:** 817–845

Palmgren MG, Baekgaard L, Lopez-Marques RL, Fuglsang AT (2011) Plasma membrane ATPases. *In* A Murphy, B Schulz, WA Peer, eds, The Plant Plasma Membrane. Springer, Berlin, pp 177–192

Pan H, Oztas O, Zhang X, Wu X, Stonoha C, Wang E, Wang B, Wang D (2016) A symbiotic SNARE protein generated by alternative termination of transcription. Nat Plants **2:** 15197

Park M, Krause C, Karnahl M, Reichardt I, El Kasmi F, Mayer U, Stierhof YD, Hiller U, Strompen G, Bayer M, et al (2018) Concerted action of evolutionarily ancient and novel SNARE complexes in flowering-plant cytokinesis. Dev Cell **44:** 500–511.e4

Rafiqi M, Gan PHP, Ravensdale M, Lawrence GJ, Ellis JG, Jones DA, Hardham AR, Dodds PN (2010) Internalization of flax rust avirulence proteins into flax and tobacco cells can occur in the absence of the pathogen. Plant Cell **22:** 2017–2032

Rayle DL, Cleland R (1970) Enhancement of wall loosening and elongation by acid solutions. Plant Physiol **46:** 250–253

Roelfsema MRG, Hedrich R (2005) In the light of stomatal opening: New insights into 'the Watergate.' New Phytol **167:** 665–691

Sanderfoot A (2007) Increases in the number of SNARE genes parallels the rise of multicellularity among the green plants. Plant Physiol **144:** 6–17

Saponaro A, Porro A, Chaves-Sanjuan A, Nardini M, Rauh O, Thiel G, Moroni A (2017) Fusicoccin activates KAT1 channels by stabilizing their interaction with 14-3-3 proteins. Plant Cell **29:** 2570–2580

Schindelin J, Arganda-Carreras I, Frise E, Kaynig V, Longair M, Pietzsch T, Preibisch S, Rueden C, Saalfeld S, Schmid B, et al (2012) Fiji: An open-source platform for biological-image analysis. Nat Methods **9:** 676–682

Schindler T, Bergfeld R, Hohl M, Schopfer P (1994) Inhibition of Golgi apparatus function by brefeldin A in maize coleoptiles and its consequences on auxin-mediated growth, cell-wall extensibility and secretion of cell wall proteins. Planta **192:** 404–413

Shimazaki K, Doi M, Assmann SM, Kinoshita T (2007) Light regulation of stomatal movement. Annu Rev Plant Biol **58:** 219–247

Shope JC, Peak D, Mott KA (2008) Stomatal responses to humidity in isolated epidermes. Plant Cell Environ **31:** 1290–1298

Sklodowski K, Riedelsberger J, Raddatz N, Riadi G, Caballero J, Chérel I, Schulze W, Graf A, Dreyer I (2017) The receptor-like pseudokinase MRH1 interacts with the voltage-gated potassium channel AKT2. Sci Rep **7:** 44611

Sondergaard TE, Schulz A, Palmgren MG (2004) Energization of transport processes in plants: Roles of the plasma membrane H^+-ATPase. Plant Physiol **136:** 2475–2482

Südhof TC, Rothman JE (2009) Membrane fusion: Grappling with SNARE and SM proteins. Science **323:** 474–477

Sutter JU, Campanoni P, Tyrrell M, Blatt MR (2006) Selective mobility and sensitivity to SNAREs is exhibited by the Arabidopsis KAT1 K^+ channel at the plasma membrane. Plant Cell **18:** 935–954

Sutter JU, Sieben C, Hartel A, Eisenach C, Thiel G, Blatt MR (2007) Abscisic acid triggers the endocytosis of the Arabidopsis KAT1 K^+ channel and its recycling to the plasma membrane. Curr Biol **17:** 1396–1402

Sze H, Li X, Palmgren MG (1999) Energization of plant cell membranes by H^+-pumping ATPases: Regulation and biosynthesis. Plant Cell **11:** 677–690

Thiel G, Blatt MR, Fricker MD, White IR, Millner P (1993) Modulation of K^+ channels in Vicia stomatal guard cells by peptide homologs to the auxin-binding protein C terminus. Proc Natl Acad Sci USA **90:** 11493–11497

Tyrrell M, Campanoni P, Sutter JU, Pratelli R, Paneque M, Sokolovski S, Blatt MR (2007) Selective targeting of plasma membrane and tonoplast traffic by inhibitory (dominant-negative) SNARE fragments. Plant J **51:** 1099–1115

Varlamov O, Volchuk A, Rahimian V, Doege CA, Paumet F, Eng WS, Arango N, Parlati F, Ravazzola M, Orci L, et al (2004) i-SNAREs: Inhibitory SNAREs that fine-tune the specificity of membrane fusion. J Cell Biol **164:** 79–88

Velasquez SM, Barbez E, Kleine-Vehn J, Estevez JM (2016) Auxin and cellular elongation. Plant Physiol **170:** 1206–1215

Vialet-Chabrand S, Hills A, Wang Y, Griffiths H, Lew VL, Lawson T, Blatt MR, Rogers S (2017) Global sensitivity analysis of OnGuard models identifies key hubs for transport interaction in stomatal dynamics. Plant Physiol **174:** 680–688

Waghmare S, Lileikyte E, Karnik R, Goodman JK, Blatt MR, Jones AME (2018) SNAREs SYP121 and SYP122 mediate the secretion of distinct cargo subsets. Plant Physiol **178:** 1679–1688

Wang Y, Noguchi K, Ono N, Inoue S, Terashima I, Kinoshita T (2014) Overexpression of plasma membrane H^+-ATPase in guard cells promotes light-induced stomatal opening and enhances plant growth. Proc Natl Acad Sci USA **111:** 533–538

Xue Y, Yang Y, Yang Z, Wang X, Guo Y (2018) VAMP711 is required for abscisic acid-mediated inhibition of plasma membrane H^+-ATPase activity. Plant Physiol **178:** 1332–1343

Yamauchi S, Takemiya A, Sakamoto T, Kurata T, Tsutsumi T, Kinoshita T, Shimazaki K (2016) The plasma membrane H^+-ATPase AHA1 plays a major role in stomatal opening in response to blue light. Plant Physiol **171:** 2731–2743

Yang H, Murphy A (2013) Membrane preparation, sucrose density gradients and two-phase separation fractionation from five-day-old Arabidopsis seedlings. Bio-protocol **3:** e1014

Yoshida S, Uemura M, Niki T, Sakai A, Gusta LV (1983) Partition of membrane particles in aqueous two-polymer phase system and its practical use for purification of plasma membranes from plants. Plant Physiol **72:** 105–114

Zhang B, Karnik R, Wang Y, Wallmeroth N, Blatt MR, Grefen C (2015) The Arabidopsis R-SNARE VAMP721 interacts with KAT1 and KC1 K^+ channels to moderate K^+ current at the plasma membrane. Plant Cell **27:** 1697–1717

Zhang B, Karnik R, Donald N, Blatt MR (2018) A GPI signal peptide-anchored split-ubiquitin (GPS) system for detecting soluble bait protein interactions at the membrane. Plant Physiol **178:** 13–17

Zhang X, Wang H, Takemiya A, Song CP, Kinoshita T, Shimazaki K (2004) Inhibition of blue light-dependent H^+ pumping by abscisic acid through hydrogen peroxide-induced dephosphorylation of the plasma membrane H^+-ATPase in guard cell protoplasts. Plant Physiol **136:** 4150–4158